Tissue architecture delineates field cancerization in BRAF^{V600E}-induced tumor development

Elin Schoultz[1*], Ellen Johansson[1*], Carmen Moccia[1], Iva Jakubikova[1], Naveen Ravi[2], Shawn Liang[1], Therese Carlsson[1], Mikael Montelius[3], Konrad Patyra[4], Jukka Kero[4], Kajsa Paulsson[2], Henrik Fagman[1,5], Martin O. Bergo[6], Mikael Nilsson[1**]

*contributed equally to the study

**Corresponding author: mikael.nilsson@gu.se

[1]Sahlgrenska Center for Cancer Research, Institute of Biomedicine, University of Gothenburg, SE-40530, Göteborg, Sweden

[2]Division of Clinical Genetics, Department of Laboratory Medicine, Lund University, Lund, SE-22184, Sweden

[3]Department of Radiology, Institute of Clinical Sciences, University of Gothenburg, SE-41345, Göteborg, Sweden

[4]Department of Endocrinology, University of Turku, Åbo, FI-20521, Finland

[5]Department of Clinical Pathology, Sahlgrenska University Hospital, Göteborg, SE-41345, Sweden

[6]Department of Biosciences and Nutrition, Karolinska Institute, Huddinge, SE-14183, Sweden

Present address:

Iva Jakubikova, Diabetes Centre, Institute for Clinical and Experimental Medicine, Prague, Czech Republic; Faculty of Medicine, Charles University, Hradec Kralove, Czech Republic;

Carmen Moccia, EMBL Barcelona, Career del Dr. Aiguader 88, Barcelona, Spain

Summary statement

This study investigates how a BRAF-mutant lineage becomes a cancerized lineage by escaping cell competition from non-mutant cells in a mouse model of sporadic thyroid cancer development.

Abstract

Cancer cells hijack developmental growth mechanisms but whether tissue morphogenesis and architecture modify tumorigenesis is unknown. Here, we characterized a new mouse model of sporadic thyroid carcinogenesis based on inducible expression of $BRAF^{V600E}$ from the thyroglobulin promoter (*TgCreER*^{T2}). Spontaneous activation of this *Braf*-mutant allele due to leaky CRE activity revealed that intrinsic properties of thyroid follicles determined BRAF-mutant cell fate. Papillary thyroid carcinomas developed multicentrically within a normal microenvironment. Each tumor originated from a single follicle that provided a confined space for growth of a distinct tumor type. Lineage tracing revealed oligoclonal tumor development in infancy and early selection of $BRAF^{V600E}$ kinase inhibitor-resistant clones. Somatic mutations were few, non-recurrent, and limited to advanced tumors. Female mice developed larger tumors than males, reproducing the gender difference of human thyroid cancer. These data indicate that $BRAF^{V600E}$-induced tumorigenesis is spatiotemporally regulated depending on the maturity and heterogeneity of follicles. Moreover, thyroid tissue organization seems to determine whether a *BRAF*-mutant lineage becomes a cancerized lineage. The sporadic thyroid cancer model provides a new tool to evaluate drug therapy at different stages of tumor evolution.

Introduction

The cell of origin in differentiated thyroid cancer – the follicular cell – gives rise to two major tumor types: follicular thyroid carcinoma (FTC) and papillary thyroid carcinoma (PTC), both overrepresented in women (Dralle et al., 2015; Williams, 2015). As indicated by the nomenclature, FTC and PTC possess different features of tumor growth and differentiation that influence clinical outcome and are therefore considered as separate cancer entities (Dralle et al., 2015). The fact that *RAS* (mainly *NRAS*) and *BRAF* mutations predominantly associate with FTC and PTC, respectively (Howell et al., 2013; Xing, 2005) suggests that mutation identity might influence morphogenesis of a distinct carcinoma phenotype. However, these driver mutations occur, although with varying frequencies, in nearly all thyroid cancer types. For example, $BRAF^{V600E}$-induced PTC comprises several subtypes including the follicular variant (Afkhami et al., 2016). A single PTC tumor may also display a mixture of growth patterns, the predominant being decisive for diagnostic subtyping. Most PTCs have a low somatic mutation burden indicating that genomic instability is not a critical factor except in advanced tumor stages (Cancer Genome Atlas Research, 2014). Although transcriptional profiling distinguishes PTC as "*RAS*-like" and "*BRAF*-like" neoplasms with different levels of tumor dedifferentiation and aggressiveness (Cancer Genome Atlas Research, 2014), the underlying mechanisms of the morphogenetic traits that give rise to heterogeneous tumor phenotypes in the thyroid are unknown.

Tumor heterogeneity conceptually implies diversification of cancer cell properties – genetically, morphologically and biochemically – involved in tumor progression. According to the clonal evolution model (Swanton, 2012), tumors arise from a single mutated cell that upon accumulation of additional somatic mutations gives rise to a tumor clone, which possesses a growth advantage. Further branched evolution of heterogeneous subclones contributes to tumor progression and provides a selection mechanism of escaping anti-cancer drug treatment (Turajlic et al., 2019). An alternative, less recognized mechanism concerns the possible involvement of a multiclonal tumor origin (Parsons, 2018), which implies that two or more independent clones cooperate in tumor development and heterogeneous tumor growth. Such clonal cooperation may be necessary for mutant cells to resist competition with non-mutant cells. Escaping surveillance mechanisms associated with normal tissue homeostasis (Bowling et al., 2019) might not only be decisive for tumor development but also influence later stages of cancer progression (Cheung et al., 2016; Echeverria et al., 2018; Reeves et al., 2018). In thyroid cancer patients, mutation analysis infers that PTC, the most common type of thyroid cancer, is a strictly monoclonal tumor (Cancer Genome Atlas Research, 2014). However, as recently reviewed (Fugazzola et al., 2020), there are several divergent reports of genetically heterogeneous tumor cell populations that argue against the prevailing concept of monoclonality, suggesting that PTC development may comprise subclonal or even oligoclonal events. Presently, there are no experimental studies addressing the clonal origin of differentiated thyroid cancer and the role of clonality in thyroid tumor development.

Mouse models have been invaluable in studies of thyroid cancer progression and evaluation of targeted therapies (Landa and Knauf, 2019). However, since conditional expression of oncogenes like mutant BRAF encompasses the majority of cells, there are no current models that reliably replicate tumor initiation and early events of the carcinogenic process within a preserved thyroid tissue microenvironment. Notably, loss of thyroid function accompanying synchronous activation of *Braf*^{CA} encoding the BRAF^{V600E} oncoprotein rapidly generates pronounced goitrous growth leading to global disruption of the normal follicular organization (Chakravarty et al., 2011), which invalidates monitoring of any discrete cellular changes presumed to characterize focal tumorigenesis. To overcome these obstacles, we adopted a novel tumorigenic approach based on spontaneous CRE-mediated recombination, which occurs at significant levels in non-induced conditions in *TgCreER*^{T2}*;Braf*$^{CA/+}$ mice that conditionally express Braf^{V600E} in the thyroid (Charles et al., 2011). This enabled us to investigate by lineage tracing the earliest stages of Braf^{V600E}-induced tumor development and elucidate the clonal origin of tumor heterogeneity. The results indicate tissue organization designated by follicle heterogeneity delimits the effective cancerization field and hence determines the fate of thyroid cells subjected to oncogene activation. Nascent follicles formed postnatally are particularly susceptible to *Braf* mutations, prone to develop oligoclonal lesions that escape competition and give rise to PTC with diverse phenotypes in mice.

Results

Spontaneous Braf^{CA} activation in mouse thyroid generates multifocally heterogeneous PTC tumors with accelerated growth in females

We crossed established *Braf^{CA}* and *TgCreER^{T2}* mouse lines (Dankort et al., 2007; Undeutsch et al., 2014) to conditionally express BRAF^{V600E} in the thyroid under control of the *thyroglobulin* (*Tg*) promoter, as previously reported (Charles et al., 2011). Unless indicated, non-induced *TgCreER^{T2};Braf$^{CA/+}$* mice devoid of tamoxifen injections were studied to elucidate whether spontaneous activation of mutant BRAF due to leaky CRE activity might reproduce sporadic thyroid cancer development. *In situ* gland volume measurements showed that the thyroid gradually increased in size, accelerating between 6 and 12 months of age in mutant animals (Figs. 1A and B). Notably, at 6 months, i.e. before great variations in thyroid size became evident, the gland was significantly larger in females than in male mutants (Fig. 1C). Consistent with stochastic generation of tumors with different growth properties, the relative enlargement of the left and right thyroid lobes differed increasingly with age in the majority of mice (Figs. 1D and E). Interestingly, 83% of 12 months old mutants (n=18) showed a higher left/right lobe ratio (Fig. 1D). The fact that larger tumors predominated in the left lobe was reinforced by a trend of the opposite lobe asymmetry in aging control animals (Fig. 1D). A single-sided preference is evident for thyroid developmental defects in both mice (Manley and Capecchi, 1995) and humans (Shabana et al., 2000), but has not previously been reported for neoplastic lesions. As documented by magnetic resonance imaging (MRI), heterogeneous tumor growth explained the lobe size differences (Figs. 1G and H; Supplementary Video 1). Mouse MRI also revealed that cystic tumors predominated peripherally whereas more solid tumor portions often had a central or medial location in the lobes.

Advanced tumor stages were further analyzed in serial-sectioned thyroids from non-induced *TgCreER^{T2};Braf$^{CA/+}$* mice between 12 and 22 months (n=15). Consistent with PTC features in humans, the tumor cells overexpressed cytokeratin 19 (Figs. 1F; Figs. S1A and B). Moreover, reminiscent of PTC subtypes classified histologically, the tumors showed a highly variable growth pattern, which comprised: i) classical or conventional PTC, with abundance of papillary formations (Figs. 1I-M; Figs. S1B and C) and the characteristic ground glass nuclei of tumor cells (Fig. 1K); ii) cystic PTC, with hobnail-like features of the epithelial lining (Fig. S1E); iii) solid variant PTC essentially devoid of papillary growth (Figs. S1G and S2A-A´); and iv) tall-cell variant PTC, with an unusual cylindrical tumor cell shape (Figs. S2D-D´). Inter- and intratumoral heterogeneity comprised altered expression levels of NKX2-1 (Figs. 1J and L-L´; Figs. S2B-B´); a key thyroid transcription factor (Fernandez et al., 2015). Notably, tumor cells invaded stroma-rich tissue either by collective migration with a preserved ability to form follicles (Figs. S1D and S2D-D´) or undergoing partial epithelial-mesenchymal transition (EMT) characterized by diminished expression and disrupted localization of E-cadherin (Figs. S1G, S2B-B´, and S2C and D). Occasionally, tumor cells infiltrated extrathyroidal tissues (Figs. S2D-D´).

Altogether, these findings indicated that sporadic activation of *Braf^{CA}* in mice generates multifocal thyroid carcinomas with distinctive growth patterns mimicking PTC subtypes in humans. Notably, the penetrance of *Braf* mutation was 100% although with highly variable tumor size and phenotypes occurring among individuals and also within the same gland, emphasizing the stochastic nature of thyroid tumorigenesis in this model. Development of larger

tumors in female mice is consistent with the well-known sex differences in occurrence of PTC (Derwahl and Nicula, 2014; Dralle et al., 2015; Rahbari et al., 2010).

$BRAF^{V600E}$-induced thyroid tumorigenesis does not require additional coding mutations

To elucidate the possible involvement of somatic mutations, tumor samples from 4-12 months old *$TgCreER^{T2}$;$Braf^{CA/+}$* mice (n=5) were subjected to whole-exome sequencing (WES). The entire lobe (age 4 months) or the most tumorous part of the lobe (age 6-12 months) was excised and sequenced; one tamoxifen-treated mutant mouse (age 4 months, induced at weaning) was included for comparison. No mutations other than *$BRAF^{V600E}$* were detected in tumors at 4 months, and few additional coding mutations (1-3 per sample) accumulated between 6-12 months (Table 1; for quality data of sequencing, see Table S1). The mutational allele fraction varied between 0.05-0.14. None of the identified mutations were recurrent, and none were previously reported in thyroid cancer with the exception of *Pclaf* (Mizutani et al., 2005). Samples subjected to WES analysis were not morphologically examined, but since neoplastic cells predominated in most investigated tumorous tissues the low allelic fraction of the identified mutations strongly suggest that they in all probability were subclonal. These data conform to previous reports indicating that most sporadic PTCs exhibit few genetic abnormalities apart from the oncogenic driver mutation (Cancer Genome Atlas Research, 2014). In the current model, it is thus evident that early tumor development does not require additional mutations in coding genes.

Follicular neoplasms with different sensitivity to BRAF^{V600E} kinase inhibition develop within a structurally and functionally preserved thyroid microenvironment

To understand the basis of heterogeneous tumor growth, earlier stages of tumor development in non-induced *TgCreER^{T2};Braf$^{CA/+}$* mice were studied. At 3 months of age, mutant thyroids displayed a limited number of abnormal follicles surrounded by follicles with normal size and shape (Fig. 2A). The enlarged follicles were of two major types: cell-rich, comprising a thickened and irregular-shaped epithelium, and hollow, consisting of flattened cells and a distended epithelial lining (Fig. 2A´), henceforth referred to, respectively, as hyperplastic type and dilated or "giant" type of follicles. On average, each lobe contained 2-3 clusters of either type of follicular abnormalities (Fig. 2B; n=10, serial-sectioned thyroids). Hyperplastic follicles were regularly embedded in the lobe interior whereas giant follicles mostly had a peripheral location. The neoplastic nature of these early alterations was confirmed by blocking mutant BRAF kinase activity with vemurafenib (PLX4720), administered from the date of weaning, which virtually abolished thyroid enlargement in 3 months old mice (Fig. 2C). Female and male thyroids showed equal numbers of hyperplastic and dilated follicles and responded similarly to vemurafenib, although the relative size reduction was more pronounced in females due to the larger glands developing in untreated mutants (Figs. 2B and C). Notably, vemurafenib inhibited giant follicle formation but did not fully prevent the generation of hyperplastic follicles and microcarcinomas distinguished by a papillary growth pattern (Fig. 2D; see further below).

Mutant thyroids also consisted of normal-sized and moderately enlarged follicles with lumens conspicuously devoid of colloid (Fig. 2A´). A similar effect was evident globally in tamoxifen-induced mice before the compensatory high serum levels of thyroid stimulating hormone (TSH) stimulated goitrous growth (Figs. S3A-C). By contrast, confirming previous notions (Charles et al., 2011), non-induced *TgCreER*^{T2}*;Braf*$^{CA/+}$ mice maintained systemic thyroid hormone homeostasis (Figs. S3C-E). This indicated that the resolution of colloid likely was TSH-independent and a direct effect of constitutive mitogen-activated protein kinase (MAPK) signaling in BRAF-mutant thyroid cells. It is previously known that thyroglobulin (TG), the thyroid prohormone and major constituent of follicular colloid, is down-regulated in BRAF^{V600E}-driven thyroid tumors, featuring a poorly differentiated state, in mice (Chakravarty et al., 2011). We confirmed this by qPCR (Table S2): induced *Braf*^{CA} activation virtually abolished thyroid-specific gene expression and diminished *Pax8*, a major transcriptional regulator of thyroid differentiation (Fernandez et al., 2015) (Table S2). By contrast, in non-induced conditions, consistent with less amounts of oncogene-activated cells, the transcription levels of *Pax8*, *Tg*, *Tpo* (thyroid peroxidase) and *Tshr* (TSH receptor) were partially reduced (Table S2). Morphologically, this corresponded to a markedly heterogeneous tissue consisting of normal follicles with homogeneous TG staining of the colloid, dilated follicles with retention of agglutinated TG in the lumen, and hyperplastic follicles lacking TG immunoreactivity (Figs. 2E and E´, left and right panels). Since microcarcinomas and manifest PTCs were also entirely TG negative (Figs. S4A and B), confirming loss of differentiation of BRAF-mutant cells, these findings suggested that abnormal follicles with retained TG expression consisted of both mutant and normal cells and did not develop into tumors. Surprisingly, *Slc5a5* encoding the sodium-iodide symporter (NIS) was equally suppressed after spontaneous and induced *Braf*^{CA} activation

(Table S2). It is difficult to explain this by other than the NIS expression being more broadly inhibited encompassing not only BRAF-mutant cells. A bystander effect specifically affecting *Slc5a5* might possibly occur related to the fact that NIS is independently regulated and more sensitive to MAPK activation than other thyroid-specific genes (Chakravarty et al., 2011; Ingeson-Carlsson and Nilsson, 2013).

These findings indicated that mouse thyroid cells respond differently to sporadic $Braf^{CA}$ activation and give rise to a heterogeneous population of follicular lesions of which only a fraction is tumorigenic. This pattern reminds of the normal follicle heterogeneity and generation of multinodular goiter on the basis of inherent variations in growth and functional properties of thyroid epithelial cells (Studer et al., 1989).

$BRAF^{V600E}$-induced loss of differentiation entails abolished CRE expression in mutant cells

The next set of experiments was undertaken to elucidate in more detail how the pre-existing thyroid tissue organization influenced $BRAF^{V600E}$-driven tumorigenesis in $TgCreER^{T2};Braf^{CA/+}$ mice. Immunohistochemistry using antibodies against human $BRAF^{V600E}$ oncoprotein was not feasible to localize and estimate the amounts of mutant cells due to high background including ubiquitous nuclear staining (data not shown). We therefore investigated whether the expression of CRE recombinase, which correlated to that of TG, might serve as a marker to distinguish normal from BRAF-mutant cells. Indeed, confirming this relationship, only follicles with normal size and colloid structure consisted predominantly of CRE+ cells whereas hyperplastic follicles and tumors were devoid of CRE immunoreactivity (Figs. 3AA´ and BB´). Moreover, dilated follicles were generally CRE negative with only few weakly positive cells observed (Fig. 3A´). It

is noteworthy that seemingly normal follicles frequently consisted of both CRE positive and negative epithelial cells (Figs. 3A´). As the expression level of TG normally varies among thyroid follicles and even between adjacent follicular cells (Sellitti and Suzuki, 2014), it is possible that cells lacking CRE expression comprise also non-mutant cells. However, presence of numerous largely CRE negative follicles empty of colloid in peri-tumorous tissue (Figs. 3B and B´, bottom) suggests that mutant cells predominated in these enlarged follicles. Coordinated loss of *Tg* and *CreER*^{T2} mRNA expression and rescue of *Tg* promoter activity by vemurafenib was confirmed with qPCR in thyroid samples from non-induced *Braf*^{CA} mice (Fig. 3C).

Altogether, these observations indicated that down-regulation of CRE accompanied loss of expression of differentiation markers in BRAF-mutant thyroid cells not only in manifest tumors and neoplastic follicles but also when present in follicles with more subtle alterations. As evidenced below, this enabled a tracing strategy to distinguish clonal fates of mutant thyroid cells with different temporal onset of spontaneous *Braf*^{CA} activation.

Tumor initiation starts perinatally by oligoclonal growth of BRAF-mutant cells delineated by the originating follicle territory

To get insight about the earliest stages of stochastic tumor development, *TgCreER*^{T2}*;Braf*$^{CA/+}$ mice were crossed with established *Cre* reporter strains. Consistent with previous findings (Undeutsch et al., 2014), specificity of tracing the thyroid follicular lineage was confirmed by induced CRE activation in *TgCreER*^{T2} mice carrying a lox-STOP-lox lacZ allele targeted to the *Rosa26* (*R26R*) locus (Soriano, 1999). The follicular epithelium of *TgCreER*^{T2}*;R26R* mice uniformly stained positive for X-gal corresponding to expression of CRE recombinase, whereas

surrounding non-thyroid tissues were unlabeled (Figs. 4A-A´). In the absence of tamoxifen, only occasional X-gal^{+} cells appeared in adult mice suggesting a low rate of spontaneous CRE-mediated recombination (Fig. 4B-B´). In similar experiments, the *mTmG* reporter designed to switch from membrane-tagged mTomato to mGFP expression upon activation was used to increase the resolution of lineage tracing (Muzumdar et al., 2007); cells expressing either of these fluorescent labels were henceforth named mT^{+} and mG^{+} cells, respectively. This revealed a gradual accumulation of mG^{+} cells from birth eventually comprising nearly 40% of the follicular cell population in adult *TgCreER^{T2};mTmG* mice (Figs. 4C and 5A). The fact that spontaneous reporter activation levelled off might relate to the accumulation of inactive follicles, comprising cells with diminished function that probably exhibit reduced *Tg* promoter activity, in aging mice (Studer et al., 1978). Nonetheless, since *mTmG* faithfully detected contiguous mG^{+} progenies of normally dividing follicular cells (Fig. 4C), we chose this reporter strain for clonal analysis of BRAF-induced tumor development.

Unlike after induction, it is conceivable that spontaneous CRE-mediated activation of multiple alleles in a given cell occurs independently and sequentially, most likely with a considerable lag time, on the basis of non-parallel recombination (Liu et al., 2013). Since we found that *Braf^{CA}* activation concomitantly down-regulated TG and CRE (Figs. 3C and 4D), this predicts that in *TgCreER^{T2};Braf$^{CA/+}$;mTmG* mice, whether the reporter gene or *Braf^{CA}* is being first activated, mutant cells become either mGFP-labelled or retain mTomato expression resulting in clonal expansion of mG^{+} or mT^{+} cell cohorts, respectively (Fig. 4E). To confirm this assumption and validate usefulness of the model in clonal tracing, serially sectioned thyroids obtained from non-

induced *TgCreER^{T2};Braf$^{CA/+}$;mTmG* mice were carefully examined from the onset of TG expression embryonically to adulthood.

The embryonic thyroid normally consists of a branching network of parenchyma in which folliculogenesis occurs from embryonic day E15.5 and onwards (Liang et al., 2018), which did not change in mutant mouse embryos (investigated at E18.5). We also found that mG-labeled cells were rare at this early stage (data not shown). However, the number of mG$^+$ cells increased postnatally (P), the majority possessing a random distribution consistent with stochastic reporter activation (Fig. S5A). Additionally, mG$^+$ cells clustered both in the pre-follicular parenchymal cords and in nascent follicles suggesting initiation of clonal expansion (Figs. 4F and G). There were no signs of abnormal follicular growth at P10.

At one month of age, the most conspicuous finding in *TgCreER^{T2};Braf$^{CA/+}$;mTmG* mice was the presence of compound mT$^+$/mG$^+$ follicles that were considerably larger than the surrounding normal-sized follicles (Figs. 4H and S5B$^{1-6}$). The dual-labelled follicles consisted of two distinctive mT$^+$ and mG$^+$ epithelial domains, mostly of equal size, that were contiguous encircling an irregular lumen (Figs. 4H and S5B$^{1-6}$). Some enlarged follicles uniformly consisted of mT$^+$ cells, whereas follicles predominated by mG$^+$ cells were only rarely observed. In 3-6 months old mice, compound follicles co-existed with similarly dual-labeled microcarcinomas consistent with coordinated expansion of mT$^+$ and mG$^+$ tumor clones (Fig.-4I). Notably, mT$^+$ and mG$^+$ portions of the tumorous epithelium were always interlinked at discrete sites indicating a shared follicle origin (Figs. 4I and S6A). Both clones thus participated in the generation of a conspicuous papillary growth pattern by means of multiple folding of the single-layered

epithelium (Figs. 4I-I´and J; Figs. S6A-C). This indicated that tumor cell proliferation virtually always occurred by planar cell division, implying that the originating epithelium maintained its apicobasal polarity and did not stratify due to a multilayering process. Tumor-associated stromal cells were sparsely present, intervening adjacent layers of the neoplastic epithelium (Figs. 4I´and S6B´).

These experiments thus enabled us to trace novel features of tumor evolution in mouse PTC confined to a single follicle origin. Neoplastic follicles developed into tumors by coordinated growth of BRAF-mutant cells in an oligoclonal fashion.

Tumor evolution involves clonal selection of cells with early onset Braf^{CA} activation

A predominance of mT^{+} cells over mG^{+} cells was evident in most tumorous lesions (Figs. 4I and S6). To estimate the overall clonal contribution, we quantified morphometrically the relative amounts of mG^{+} cells accumulating in the thyroid of *TgCreER^{T2};Braf$^{CA/+}$;mTmG* mice between postnatal day 10 (P10) and 12 months (n=27; each lobe serially-sectioned at three levels). To exclude that calculations were biased by stromal cells, the amount of which varied among lesions, only parenchymal/epithelial cells were counted. This showed that mG^{+} cell fraction never exceeded the corresponding number in age-matched *TgCreER^{T2};mTmG* controls; on the contrary, mT^{+} cells in mutants gradually increased at the expense of mG^{+} cells, which comprised less than 10% in 12 months old mutants (Fig. 5A). Moreover, although the spontaneous rate of CRE-mediated recombination was similar in both sexes (Fig. 5B), expansile mT^{+} clones predominated in female mice (Fig. 5C), consistent with the observed sex differences in tumor growth (Fig. 1C). Dual labeling analysis of individual lesions further indicated that clonal

selection in favor of mT^+ mutant cells started already during early tumor development (Fig. 5D). Accordingly, the majority of manifest PTC tumors independent of subtype consisted exclusively of mT^+ cells (Figs. 5E and F). Neoplasms solely composed of mG^+ cells were not encountered at any age.

It is noteworthy that mT^+ and mG^+ clones co-existing in a single enlarged follicle occasionally showed distinct growth characteristics (Figs. 5G and H). On the other hand, some dual labeled tumors displayed a homogeneous growth pattern for which the participating clones in fact were impossible to distinguish without clonal tracing (Figs. 5I and S6A-C). These observations further argue that the cellular response to mutant BRAF differs much among follicles.

Next, we quantified the clonal responsiveness to vemurafenib administered to *TgCreER^{T2};Braf$^{CA/+}$;mTmG* mice from weaning up to 3 months of age (Fig. S7A, top). This showed that drug treatment largely restituted *mTmG* activation (Fig. S7A, bottom). It is likely that this effect largely depended on recovery of CRE expression in BRAF-mutant cells. Accordingly, mG^+ cells accumulated in follicles that retained a normal size and shape (Figs. S7B and C), suggesting that most mutant cells maintained a quiescent state. Nonetheless, drug-treated mice occasionally developed thyroid microcarcinomas that were essentially free of mG^+ cells (Fig. S7C). This indicated that a subpopulation of mT^+ mutant cells gained a growth advantage presumably before drug administration, and that the expanding clones acquired resistance to vemurafenib already at a pre-tumorous stage.

Restricted growth response of BRAF-mutant cells co-existing with non-mutant follicular cells

The abundance of moderately enlarged follicles that fully responded to vemurafenib and yet did not develop tumors suggested that BRAF-mutant cells ceased to proliferate soon after oncogenic activation. To distinguish mutant from non-mutant cells in these follicles, 6-month-old *TgCreER^{T2};Braf$^{CA/+}$;mTmG* mice were repeatedly injected with tamoxifen 10 days before sacrifice (Fig. 6A, top). Delayed induction of CRE increased the number of mG^{+} cells to about 75% of the amounts generated by spontaneous reporter activation in control mice (Fig. 6A, bottom). This provided a reliable estimate of the relative proportions of non-mutant/responding cells and mutant/non-responding cells at 6 months. Notably, in tissue sections, the induced mG^{+} cells had a markedly heterogeneous distribution. Normal-sized follicles were either uniformly or partially labeled, whereas hyperplastic follicles, giant follicles and microcarcinomas were virtually devoid of mG^{+} cells (Figs. 6B and C). This confirmed that tamoxifen was unable to trigger reporter gene activation in neoplastic lesions, but also that seemingly normal follicles retained BRAF-mutant cells in the encircling epithelium. Of particular interest, many of the moderately enlarged follicles contained only occasional mG^{+} cells (Fig. 6D) or consisted of alternating mG^{+} and mT^{+} epithelial segments (Fig. 6E).

In this experiment, it is likely that tamoxifen induced co-activation of *Braf^{CA}* and the reporter in normal cells with maintained CRE expression. However, the lag time between injection and sacrifice was too short to generate no more than minimal changes. Moreover, all induced cells were likely encountered in the mG^{+} population. Altogether, this indicated that a large number of BRAF-mutant cells co-existing with non-mutant cells were growth-restricted and unable to elicit the entire carcinogenic cascade.

Discussion

By means of spontaneous CRE-mediated activation of oncogenic *Braf*^{CA} in the absence of tamoxifen, we were able to monitor sporadic PTC development from the earliest signs of tumor initiation in infancy to the occurrence of macroscopic tumors in adult mice. This revealed that random activation of *Braf*^{CA} in a minority of cells accumulating over time distinguished different neoplastic growth patterns depending on spatiotemporal cues inherited to the tissue organization of the thyroid. By providing a secluded microenvironment for neoplastic growth, each follicle constitutes a minimal effective tumorigenic unit. However, within a single follicle, the relationship between simultaneously occurring BRAF-mutant and non-mutant cells seems to determine whether cooperation or competition mechanisms facilitate or counteract tumorigenesis in an autonomous fashion. The follicular architecture thus identifies and delineates intrinsic boundaries of the cancerization field in the thyroid. The study also provides the first experimental insight into morphogenesis of the archetypical papillary growth pattern of PTC. Manufactured by oriented cell division, longitudinally with reference to the curved plane of the originating follicle, proliferating clones expand linearly and give rise to incremental folding of the epithelium. This growth mechanism, by which tumor cells maintain both apical polarity and a basal border towards the extrafollicular space, clearly distinguishes PTC from FTC characterized by neoplastic folliculogenesis. How such divergent tumor growth patterns arise from constitutive activation of the same signaling pathway, driven by *BRAF* and *RAS* mutations in human thyroid cancer, remains a key question.

Non-parallel recombination of *Braf*^{CA} and the *mTmG* reporter due to leaky CRE activity was instrumental in distinguishing BRAF-mutant thyroid cells of different clonal origin. A bearing concept for our conclusions is also that inducible CRE expression in this model is permanently shut-off once *Braf*^{CA} is activated, preventing further recombination events in the progeny. In support of this assumption, TG and CRE were coordinately down-regulated in mutant cells and recovered by vemurafenib (PLX4720). This confirms previous reports indicating that *Tg* promoter activity in mouse thyroid follicular cells is fully repressed as long as mutant BRAF kinase activity prevails (Chakravarty et al., 2011; Charles et al., 2011). This strong and persistent dedifferentiating effect with reference to thyroid function probably relates to the fact that activation of the MAPK signaling pathway by BRAF^{V600E}, unlike that of constitutively active RAS, resists feedback inhibition (Pratilas et al., 2009). It is therefore conceivable that any TG/CRE positive cells occasionally present in neoplastic lesions likely comprised entrapped normal cells. Although we cannot technically exclude that some tumor cells retained TG expression and the possibility of being subclonally labeled due to leaky CRE, it is highly unlikely that *mTmG* activation coincided with the initiation of a putative subclone with different growth features. Moreover, if reporter activation occurred subclonally it would likely generate a more random mG^{+} labeling than was evident in most neoplastic lesions. In fact, induced reporter activation by delayed tamoxifen administration virtually labeled only follicular cells that exhibited no signs of clonal growth. It is thus conceivable that in our working model, progenies of mG^{+} ancestral mutant cells are inevitably labelled simply due to reporter gene activation occurred before that of *Braf*^{CA}, and that mT^{+} tumor clones are unable to undergo further CRE-mediated recombination events after *Braf*^{CA} is activated (Fig. 4E).

The most conspicuous finding of our dual reporter tracing experiments was the oligoclonal nature of individual tumors. This was unexpected in view of current understanding that PTC in humans is a monoclonal disease. The concept of monoclonality of PTC relies mainly on genomic analysis from the TCGA study (Cancer Genome Atlas Research, 2014; Ghossein et al., 2013) and paired sequencing of primary tumors and distant metastases (Giannini et al., 2007; Gopal et al., 2018; Ricarte-Filho et al., 2009), indicating that the identity of genetic drivers are mutually exclusive and maintained during cancer progression in the majority of cases. However, the bulk of information on intratumor genetic heterogeneity characterizing earlier PTC stages, recently reviewed by Fugazzola et al (Fugazzola et al., 2020), call for an unbiased evaluation of this controversial issue. More specifically, findings of a heterogeneous distribution of *BRAF* mutation confined to a subset of tumor cells in small-size tumors (de Biase et al., 2014; Finkel et al., 2016) suggest that monoclonality for *BRAF* predominating in more advanced tumor stages of PTC might be the result of tumor evolution. Inconsistent immunostaining for $BRAF^{V600E}$ protein expression in a minority of manifest PTCs (Cancer Genome Atlas Research, 2014; Ghossein et al., 2013) are in line with this possibility. Our findings of a growth advantage of mT^{+} tumor clones outrivaling mG^{+} clones over time provide the first experimental proof of clonal selection during tumorigenesis of differentiated thyroid cancer in a mouse model. In humans, a homogeneous pattern of X chromosome inactivation (XCI) in tumor cells that characterize and distinguish individual tumor loci of multifocal PTCs (Shattuck et al., 2005) is often referred to refuting an oligoclonal origin of thyroid cancer. However, patch size confined to the progeny of a single precursor cell inheriting the same XCI pattern is so large in human thyroid tissue that assessment of clonality on this basis is doubtful (Jovanovic et al., 2003; Novelli et al., 2003).

Homotypic expression of X-linked markers may in fact conceal a multiclonal tumor origin from detection (Garcia et al., 2000; Parsons, 2018).

As documented in studies on aggregation chimeras of *Apc* mutant mice, a multi- or polyclonal tumor origin is evident in hereditary intestinal cancer (Halberg and Dove, 2007). In this model, recruitment by facilitating transformation of neighboring crypt cells rather than cooperation of two independent progenitors appears necessary to thrive tumor growth (Thliveris et al., 2013). A similar recruitment mechanism characterizes a mouse skin cancer model in which pre-malignant lesions develop polyclonally but the arising carcinoma evolves through a clonal sweep favoring the *Hras* mutant tumor-initiating cells (Reeves et al., 2018). In the present study, we cannot exclude the possibility that non-mutant thyroid follicular cells similarly might contribute to phenotypic changes elicited by $Braf^{CA}$ activation. However, the experiments with delayed induction with tamoxifen showed that responding normal cells co-existed with mutant cells in the same follicle without signs of clonal expansion, arguing against recruitment as a predominant factor. Moreover, neoplastic lesions almost exclusively consisted of cells that failed to recombine *mTmG* indicating homogeneous $Braf^{CA}$ activation. The heterogeneous growth pattern of oligoclonal thyroid tumors, distinguished by lineage tracing, rather indicated that participating clones likely had a dual ancestral mutant cell origin.

In view of the fairly high spontaneous rate of CRE-mediated recombination in $TgCreER^{T2}$ mice, eventually comprising the majority of follicles and several cells in each, the number of overt tumors encountered in adult $TgCreER^{T2};Braf^{CA}$ mice were surprisingly few. Assuming that CRE recombines $Braf^{CA}$ and *mTmG* alleles with similar efficiencies, available flow cytometry data

obtained from studies in normal mice (Gawade et al., 2016) extrapolates that approximately 16,000 thyroid cells expressed mutant BRAF in adult mutants. Even if this figure might be an overestimation, it is conceivable that only a small percentage of primarily BRAF-mutant cells were fully transformed and capable of generating tumors in the current model. From this follows that most follicular cells resist oncogenic activation by mutant BRAF, suggesting an intriguing possibility that mouse thyroid tissue possesses a natural ability to restrain the behavior of precancerous cells. Such tumor-suppressive signals may serve to maintain epithelial differentiation and tissue homeostasis (Bissell and Hines, 2011), e.g. by discarding potentially harmful cells by apical extrusion (Kon et al., 2017; Vermeulen et al., 2013). Intrinsic surveillance mechanisms probably explain why no tumors developed after *Braf*^{CA} activation in a fraction of thyroid cells mediated by viral vectors administered directly into the adult gland (Shimamura et al., 2013). Using another *Cre* driver that mediated a higher transformation efficiency, intrathyroidal vector injections generated PTC with phenotypic characteristics similar to the present findings although with a much delayed onset (Shimamura et al., 2018). This suggests that enhanced BRAF^{V600E} expression is sufficient to overmaster the natural protection against oncogenic insults prevailing in the mouse thyroid. Further characterization of tumor heterogeneity development in the current model might be accomplished by adopting BaseScope *in situ* detection of driver point mutations at single cell resolution, as recently developed for human tumor tissues (Baker et al., 2017).

Consistent with Mina Bissell´s dictum "the phenotype is dominant over the genotype of even tumor cells" explaining the dormancy of occult tumors (Bissell and Hines, 2011), normal thyroid follicular cells thus appear to exert a stabilizing influence on the quiescent status of a neighboring cell carrying a potentially oncogenic mutation. This raises the obvious question: which cellular mechanism(s) overcome the protective role of the microenvironment provided by mature follicles to elicit tumorigenesis in the thyroid? TSH have been shown to recover BRAF-mutant cells from oncogene-induced senescence (Zou et al., 2016), presumably related to the fact that supraphysiological levels of TSH is mitogenic and stimulates thyroid cell proliferation. A related clue, supported by the present work, may be sought for in the dynamic period of thyroid development. Independent observations indicate that immature thyroid cells are more susceptible to transformation than adult cells, presumably related to a high mitotic rate in infancy in comparison to replicative senescence prevailing in the adult gland (Coclet et al., 1989); this in fact correlates to the risk of developing thyroid cancer after radiation exposure (Saad et al., 2006). As evidenced by the surge of childhood PTCs reported after the Chernobyl fallout in 1986 (Williams, 2008), this relationship probably explains the remarkably high radiosensitivity of the thyroid gland in children. Based on data obtained from ultrasound screening implemented after the Fukushima nuclear accident (Yamashita and Suzuki, 2013), there is now compelling evidence to suggest that tumor initiation of sporadic PTC occurs much earlier than previously recognized (Williams, 2015). Notably, *BRAF* mutations predominate in PTCs of the young Japanese population, which thus differ genetically from radiation-induced thyroid cancer (Mitsutake et al., 2015). On this basis, a revised hypothesis for thyroid carcinogenesis in humans is proposed (Williams, 2015), arguing that tumor initiation starts already in infancy and that

microcarcinomas may be dormant for decades or remain undiagnosed, as evident from autopsy materials (Harach et al., 1985).

We believe the present study provides direct experimental support in favor of Williams´ hypothesis. The earliest signs of dual-labeled pre-neoplastic lesions coincided with perinatal folliculogenesis. Notably, normal follicles are polyclonal by nature (Ma et al., 2010; Novelli et al., 2003; Thomas et al., 1989), arising from multiple precursor cells that assemble during the final stage of thyroid morphogenesis (Nilsson and Fagman, 2017). A foundation for developing oligoclonal tumors thus exists in newly-formed follicles. It is important to also consider that *in vivo* naïve thyroid progenitors start to differentiate before a follicle lumen is discernible (Liang et al., 2018). Retention or not of TG in the lumen of neoplastic lesions, as evident in the present study, thus provides a plausible means to estimate the fate of BRAF-mutant cells with temporally different onset of oncogenic activation; lesions entirely devoid of TG may have been initiated already at a pre-follicular stage cells whereas TG-containing lesions, which rarely progressed to cancer, most likely emerged from mature follicles. A related issue concerns recruitment of cells forming a follicle. As assembly of a basement membrane is required for folliculogenesis (Villacorte et al., 2016), it can be assumed that once an enclosing basement membrane is established no more cells from outside can join in, and all cells populating a single follicle likely descend from few, perhaps only two, initiating progenitor cells (Nilsson and Fagman, 2017). From this follows that the earlier a driver mutation is activated the greater the chance of obtaining a growth advantage over non-mutant cells present in the same follicle. Oncogenic co-activation of immature cells and clonal cooperation of growth, put into effect at a critical phase of thyroid development, might thus facilitate tumor initiation by escaping the redundancy of

normal cells in mature follicles. In the present model, the documented growth advantage of mT^+ tumor clones, requiring only one recombination event, may also be related to early onset of oncogenic activation.

The prevalence of mutations potentially contributing to carcinogenesis in normal thyroid tissue is unknown. However, the fact that PTC frequently is multifocal with independent clonal origin of individual lesions (Giannini et al., 2007; Lu et al., 2016; Shattuck et al., 2005), and that *BRAF* mutation comprises 50% or more of all PTC cases (Howell et al., 2013; Xing, 2005), argues that the sporadic mutational rate is significant. It is noteworthy that multicentric PTCs diagnosed in a single individual are often classified as distinct histopathological variants (Howell et al., 2013; Xing, 2005). In the current model, most PTC subtypes were evident in 12 months or older mutant mice suggesting that subclonal events might be involved. However, at least the classical and cystic PTC variants could be traced back to neoplastic follicles with different properties and distribution in young animals. This suggests that the natural follicle heterogeneity might influence the pattern of BRAF-driven tumor growth similar to that of multinodular goiter development (Kopp et al., 1994; Peter et al., 1985). To get further insight, it may be important to consider that thyroid cells do not respond uniformly to goitrogenic stimulation, which constrains growth to susceptible follicles or even growth-prone segments of the follicular epithelium (Smeds et al., 1987). The foundation of a differential growth response is probably generated embryonically as thyroid progenitor cells with a high intrinsic growth rate separate from cells that undergo differentiation (Liang et al., 2018). It is assumed that segregation of cells with different growth properties during development generates follicles with different size and tissue distribution in the adult gland (Nilsson and Fagman, 2013). Developmental trajectories that

govern follicle heterogeneity might thus add to the factors that modify cellular responses to mutant BRAF in the mouse thyroid. Validity of this hypothesis gains support from recent multicolor lineage tracing of xenografted colorectal cancer cells indicating that clone location and tissue geometry may contribute to heterogeneous clonal expansion (van der Heijden et al., 2019).

A female bias in thyroid tumor formation is evident in mice with conditional *Pten* inactivation (Antico-Arciuch et al., 2010; Yeager et al., 2007). This model is characterized by goiter and susceptibility to develop thyroid cancer due to increased signaling of the PI3K/AKT pathway, which sidelines the natural retardation of thyroid growth by an estrogen-dependent mechanism. Of particular interest, co-inactivation of *Pten* and *Cdkn1b* encoding p27KIP, a cyclin-dependent kinase inhibitor, further accelerated thyroid growth similar for both sexes (Antico-Arciuch et al., 2010), which suggests that stimulation of thyroid cell proliferation above a certain level abolishes any possible gender-based differences. In accordance with this notion, there are no sex differences in the penetrance, latency or severity of PTC in mice with constitutive $Braf^{CA}$ activation (Franco et al., 2011). The present study, indicating that $BRAF^{V600E}$ expression in a minority of cells generates larger thyroid tumors in females than in males, conforms with this concept. Our findings further suggest that tissue microenvironment, possibly involving local interplay of BRAF-mutant and non-mutant cells, modifies thyroid tumor development through the action of estrogen or other sex-related factors.

In summary, we provide a new mouse model for understanding the earliest stages of sporadic cancer development in the thyroid gland, and uncover *in vivo* mechanisms related to tissue maturation and architecture that restrain or markedly modify the oncogenic response. In this model, spontaneous CRE-mediated recombination formed the basis of stochastic $Braf^{CA}$ activation mediating random expression of $BRAF^{V600E}$ in few cells one at the time. As a result, the prevalence of BRAF-mutant thyroid cells slowly increased from the onset of functional differentiation and folliculogenesis in embryonic life to eventually accommodate the majority of mature follicles in adults. Concurrent observations of constrained and promoted tumorigenesis arising independently but in close proximity in mouse thyroid tissue are consistent with a heterogeneous response to mutant BRAF depending on spatiotemporal factors (Fig. 7). The key of understanding this is the autonomous nature of thyroid follicles consisting of a defined number of epithelial cells related to follicle size; what takes place in one follicle does not directly influence the neighboring ones. This means that the fate of a follicular cell carrying a potentially oncogenic mutation relies on its ability to overcome surveilling mechanisms mediated by non-mutant cells confined to the originating follicle (Fig. 7A). From this follows that coincidental activation of multiple mutant cells as follicles are about to form would stand a much better chance of initiating tumor development than a single mutant cell residing in the follicular epithelium predominated by normal cells (Fig. 7B). We also find evidence of a clonal foundation of inter- and intratumor heterogeneities, shedding light on the puzzling issue how PTC subtypes designated by distinct histopathological features might develop from lesions with identical driver mutations. Divergent growth patterns can be traced back to the follicle origin suggesting that properties inherent to the generation of natural follicle heterogeneity influence tumor

development (Fig. 7C). Clonal selection and subclonal genetic alterations may further modify the generation of tumor phenotype diversity in differentiated thyroid cancer.

Materials and Methods

Mouse lines and treatments

TgCreER^{T2} mice with inducible CRE under control of the *Tg* promoter (Undeutsch et al., 2014) were crossed with *Braf*^{CA} mice (Dankort et al., 2007) to generate *TgCreER*^{T2}*;Braf*$^{CA/+}$ mice. Both *Cre* lines were crossed with *Rosa26R* and *mTmG* reporter mice for lineage tracing, as described (Muzumdar et al., 2007; Soriano, 1999). Strains were backcrossed with C57BL/6J mice at least 10 generations before recombination. Tail tips were sampled for genotyping with PCR. Tamoxifen dissolved in sunflower oil (10 mg/ml) was injected intraperitoneally (50 µl) daily x4 for CREER^{T2} induction. Vemurafenib (PLX4720; 417 ppm) and control dietary pellets (both provided by Plexxikon) were continuously supplied during treatment period. Animal experiments were approved by the regional ethic committee (Dnr 26-2013 and Dnr 5.8.18-03925/2018) according to European standards and national regulations provided by the Swedish Agriculture Agency.

Histology, X-gal staining, immunohistochemistry and fluorescence microscopy

After sacrifice, thyroids excised *en bloc* with the trachea, esophagus and muscles were fixed in 4% paraformaldehyde and processed for paraffin sections and routine hematoxylin–eosin staining. For X-gal staining, fixed samples were washed in 2 mM MgCl2, 0.1% sodium deoxycholate, 0.02% Nonidet P-40 in PBS, pH 7.3 (washing buffer), incubated overnight at 37°C in 7.2 mM NaCl, 5 mM K3Fe(CN)6, and 5 mM K4Fe(CN)6, X-gal (Sigma Aldrich)

dissolved in washing buffer (X-gal staining solution), washed again and post-fixed before paraffin embedding. For IHC, deparaffinized sections were subjected to epitope retrieval by PT Link (Dacocytomation) and quenching of endogenous peroxidase activity prior to immunostaining optimized with the Dako EnVision system for antibodies (number/titer) against: thyroglobulin (A0251/1:5000; Dakocytomation), CRE recombinase (15036/1:125; Cell Signaling), cytokeratin-19 (ab133496/1:1800; Abcam) and NKX2-1 (PA0100/1:1000; BioPat); and the Rat Impress system for anti-E-cadherin/CDH1 (13-1900/1:4000; Novex, Life Technologies). IHC against human $BRAF^{V600E}$ was performed in both acidic and basic conditions according the manufacturers´ instructions for: VE1 (1:100-1:500; Spring Bioscience) and RM8 (1:100-1:500; Sigma Aldrich). Sections were viewed and imaged in an Olympus BX45TF microscope equipped with a Nikon DS-U2 camera. For evaluation of *mTmG* activation, fixed tissue samples were incubated in 30 % sucrose overnight, embedded in OCT Tissue-Tek (Sakura, Zoeterwoude, The Netherlands) and saved at -80°C. Cryosections were collected on Super Frost glass slides (Vector, Burlingame, MA) and counter-stained with DAPI nuclear stain (Sigma-Aldrich) before mounting with fluorescence mounting medium (Dakocytomation). Fluorescence was analyzed in a Zeiss Axioskop2 plus microscope equipped with a Nikon DS-Qi1Mc camera. Image acquisition and processing used the NIS Elements Imaging Software.

Quantitative Real-time PCR (qPCR)

Mouse thyroid samples stored at -80° C in RNA later (Thermo Fisher Scientific) were homogenized with Tissuelyser II (Qiagen) and RNA extracted using the RNeasy mini kit (Qiagen) according to manufacturer's instructions. Final RNA amounts were determined spectrophotometrically (NanoDrop1000; Thermo Scientific) after which cDNA was synthesized

using TATAA GrandScript cDNA Synthesis Kit (TATAA Biocenter) and T100 Thermal Cycler (Bio-Rad) and stored at -20°C. Primers to mouse *Tg* (forward: CATGGAATCTAATGCCAAGAACTG; reverse: TCCCTGTGAGCTTTTGGAATG), *Slc5a5* (forward: TCCACAGGAATCATCTGCACC; reverse: CCACGGCCTTCATACCACC), *Tpo* (forward: CAAAGGCTGGAACCCTAATTTCT; reverse: AACTTGAATGAGGTGCCTTGTCA), *Tshr* (forward: TCCCTGAAAACGCATTCCA; reverse: GCATCCAGCTTTGTTCCATTG), *Pax8* (forward: GATAGGAGACTACAAGCGGCA; reverse: CGGATGATTCTGTTGATGGAGC), *Era1* (forward: AGGGAAATCTTGAGCCCCTA ; reverse: ACACACCCTACAGCCCTCAT) and ER^{T2} (forward: ATGATTGGTCTCGTCTGGCG; reverse: CCAGGAGCAAGTTAGGAGCAA) were designed applying Primer-BLAST (Ye et al., 2012) based on sequences retrieved from public databases (Ensembl or Santa Cruz Genome Browser). BLAST analysis verified that the selected primer sequences were sufficiently different from the rest of the mouse transcriptome. *In silico* oligonucleotide secondary structure prediction was performed with NetPrimer (PREMIER Biosoft International). Specificity of primers was confirmed by agarose gel electrophoresis of amplicons. A reference gene panel for mouse (TATAA Biocenter) was evaluated with NormFinder; *Gapdh* was chosen as optimal reference gene based on predefined software criteria for relative quantification. Quantitative real-time PCR (qPCR) was performed with CFX384 Touch real-time cycler (Bio-Rad) and TATAA SYBR GrandMaster Mix (TATAA Biocenter) using 400 nM primer and 2 µl cDNA. Formation of expected PCR products was confirmed by agarose gel electrophoresis and all samples were analyzed by melting curve analysis.

Morphometry

The thyroid gland *in situ* (n=82) was photographed together with a ruler with an iPhone6 in-built camera. Lobe longitudinal and transverse diameters were measured with a digital slide gauge. Lobe volume was calculated using the standard formula for ellipsoids, $e = Height\ x\ Width\ x\ Depth\ x\ \frac{\pi}{6}$, as reported (van Isselt et al., 2003). Transverse diameter was used to estimate depth of the same lobes. The percentage of mG^+ thyroid cells was quantified on cryosections of thyroids (n=87) from *TgCreER^{T2};mTmG* and *TgCreER^{T2};Braf$^{CA/+}$;mTmG* mice. Specimens were serial-sectioned transversely encompassing the entire gland or at three standardized levels (equator and halfway to either lobe pole) in different experiments. Cell counting followed a systematic, unbiased protocol at x20 magnification.

Serum TSH and total T4 measurements

Blood samples drawn from the heart at sacrifice of animals were after clotting centrifuged 1800 rpm at 4°C for 10 minutes and serum collected. Thyroxine (T4) was analyzed using total T4 ELISA kit (cat. code: DNOV054, NovaTec, Germany). Absorbance was measured at 450 nm with the Wallac 1420 Victor2 (Perkin Elmer, MA, USA). The T4 concentration was calculated with MultiCalc 2000 software. Thyroid-stimulating hormone (TSH) was analyzed with the MILLIPLEX MAP Mouse Pituitary Magnetic Bead Panel (cat. code: MPTMAG-49K, Merck Millipore, Germany). Fluorescence intensity was measured with the Luminex 200 device (Austin, TX, USA) and data were analyzed with Luminex Xponent software v. 3.1.

Magnetic resonance imaging (MRI)

Mouse MRI data were acquired using a 7T horizontal bore pre-clinical MR system with a 72-mm volume coil (Bruker BioSpin MRI GmbH, Germany; software: ParaVision 5.1), and a 4-channel array rat brain receiver coil for signal reception (RAPID Biomedical GmbH, Germany). Animals were imaged in supine position and kept under anesthesia using air, oxygen and isoflurane (2-3%, Isoba vet. Schering-Plough Animal-health, Denmark). A circulating warm water and heating pad system maintained the body temperature, and a pressure sensitive pad monitored breathing (SA Instruments, Inc., NY, USA). Anatomical MR neck scans were acquired using a T2 weighted 2D RARE sequence with fat suppression (Repetition time: 4500 ms, Echo time: 35 ms, Number of averages: 16, Turbo factor: 6, Slice thickness/gap: 0.6/0.6 mm, Number of slices: 40, Pixel dimensions: 160 × 160 μm^2, Field-of-view: 2.3 × 1.6 cm^2). Following 1st & 2nd order automatic shimming, diffusion weighted images (DWI) were acquired using the SE-EPI sequence (Repetition time: 3000 ms, Echo time: 21 ms, Number of averages: 3, Slice thickness/gap: 1.0/1.5 mm, Number of slices: 3, Pixel dimensions: 311 × 318 μm^2, Field-of-view: 2.8 × 1.5 cm^2: b-values: 0, 5, 10, 20, 35, 50, 75, 100, 200, 400, 600 and 800 s/mm^2: bandwidth: 300 kHz). ADC maps were created online using mono-exponential fitting to data from all b-values.

Whole exome sequencing (WES)

Genomic DNA was extracted with All prep DNA/RNA kit (Qiagen, Hilden, Germany) and sheared via sonication using a S220 focused-ultrasonicator (Covaris, Woburn, MA) from the thyroids and kidneys, used as reference tissue, of mutant mice (n=5). DNA libraries were constructed using the SureSelectXT Mouse All Exon kit (Agilent Technologies, Santa Clara,

CA) and sequenced using Illumina's High Output Kit (150 cycles) on a NextSeq500 (Illumina, San Diego, USA) with an average depth of 140x for tumor and 70x for normal (kidney) samples. Raw reads were mapped on the mouse reference genome GRCm38 with the BWA-MEM algorithm (Li and Durbin, 2009). Picard **(**http://broadinstitute.github.io/picard) was used to remove PCR duplicates and local realignment was performed using GATK (McKenna et al., 2010). Somatic mutations were identified using MuTect2 (Cibulskis et al., 2013) with default settings using kidney as matched normal sample. Annotation of variants were carried out with ANNOVAR (Wang et al., 2010). The list of somatic mutations was filtered for a minimum coverage of 10 reads, keeping only non-synonymous mutations that were supported by ≥ 4 reads. For validation by targeted sequencing, primers were designed using the Primer3 software (http://bioinfo.ut.ee/primer3/). PCR was performed according to standard methods and libraries were constructed using the Nextera XT DNA Library Preparation Kit (Illumina, San Diego, CA, USA). Constructed libraries were sequenced on a NextSeq500 (Illumina). Raw reads were mapped on the mouse reference genome GRCm38 with BWA-MEM algorithm (Li and Durbin, 2009). Picard **(**http://broadinstitute.github.io/picard) was used to remove PCR duplicate and local realignment around the indel region was performed using GATK (McKenna et al., 2010). Somatic mutations were identified using Varscan (Koboldt et al., 2009).

Deposited WES data accessible at: http://www.ncbi.nlm.nih.gov/bioproject/606442

Statistics

Statistical analyses were made using Prism 7 for Mac Os X version 7.0 (GraphPad Software, Inc.). Analyses included unpaired t-tests assuming Gaussian distribution with graph error bars displaying mean ± standard deviation (SD). A p-value below 0.05 was considered statistically significant.

Acknowledgements

We thank David Bryder for valuable comments on the manuscript. Animal experiments were carried out at Experimental Biomedicine (EBM) and the mouse MRI unit at Sahlgrenska Academy, University of Gothenburg.

Author contributions

Study design (MN, JK and MOB), experiments (ES, EJ, CM, IJ, NR, SL, TC, MM and KP), evaluation (JK, KP, HF, MOB and MN), and writing (MN, with contributions from ES, MM, KP, HF and MOB).

Competing interests

No competing interests declared.

Funding

The study was supported by grants from the Swedish Cancer Society (2017-0657 to MN; 2016-497 to KP), the Swedish Research Council (2016-02360 to MN; 2016-01459 to KP), the Center for Innovative Medicine (to MOB), Strategic Research Area Cancer at Karolinska Institute (to

MOB), BioCare (to KP), the Gothenburg Medical Society (to ES and EJ), the Assar Gabrielsson Foundation (to ES, EJ and SL) and the ALF agreement at Sahlgrenska University Hospital (to HF).

References

Afkhami, M., A. Karunamurthy, S. Chiosea, M.N. Nikiforova, R. Seethala, Y.E. Nikiforov, and C. Coyne. 2016. Histopathologic and Clinical Characterization of Thyroid Tumors Carrying the BRAF(K601E) Mutation. *Thyroid* 26:242-247.

Antico-Arciuch, V.G., M. Dima, X.H. Liao, S. Refetoff, and A. Di Cristofano. 2010. Cross-talk between PI3K and estrogen in the mouse thyroid predisposes to the development of follicular carcinomas with a higher incidence in females. *Oncogene* 29:5678-5686.

Baker, A.M., W. Huang, X.M. Wang, M. Jansen, X.J. Ma, J. Kim, C.M. Anderson, X. Wu, L. Pan, N. Su, Y. Luo, E. Domingo, T. Heide, A. Sottoriva, A. Lewis, A.D. Beggs, N.A. Wright, M. Rodriguez-Justo, E. Park, I. Tomlinson, and T.A. Graham. 2017. Robust RNA-based in situ mutation detection delineates colorectal cancer subclonal evolution. *Nat Commun* 8:1998.

Bissell, M.J., and W.C. Hines. 2011. Why don't we get more cancer? A proposed role of the microenvironment in restraining cancer progression. *Nat Med* 17:320-329.

Bowling, S., K. Lawlor, and T.A. Rodriguez. 2019. Cell competition: the winners and losers of fitness selection. *Development* 146:

Cancer Genome Atlas Research, N. 2014. Integrated genomic characterization of papillary thyroid carcinoma. *Cell* 159:676-690.

Chakravarty, D., E. Santos, M. Ryder, J.A. Knauf, X.H. Liao, B.L. West, G. Bollag, R. Kolesnick, T.H. Thin, N. Rosen, P. Zanzonico, S.M. Larson, S. Refetoff, R. Ghossein, and J.A. Fagin. 2011. Small-molecule MAPK inhibitors restore radioiodine incorporation in mouse thyroid cancers with conditional BRAF activation. *J Clin Invest* 121:4700-4711.

Charles, R.P., G. Iezza, E. Amendola, D. Dankort, and M. McMahon. 2011. Mutationally activated BRAF(V600E) elicits papillary thyroid cancer in the adult mouse. *Cancer Res* 71:3863-3871.

Cheung, K.J., V. Padmanaban, V. Silvestri, K. Schipper, J.D. Cohen, A.N. Fairchild, M.A. Gorin, J.E. Verdone, K.J. Pienta, J.S. Bader, and A.J. Ewald. 2016. Polyclonal breast cancer metastases arise from collective dissemination of keratin 14-expressing tumor cell clusters. *Proc Natl Acad Sci U S A* 113:E854-863.

Cibulskis, K., M.S. Lawrence, S.L. Carter, A. Sivachenko, D. Jaffe, C. Sougnez, S. Gabriel, M. Meyerson, E.S. Lander, and G. Getz. 2013. Sensitive detection of somatic point mutations in impure and heterogeneous cancer samples. *Nat Biotechnol* 31:213-219.

Coclet, J., F. Foureau, P. Ketelbant, P. Galand, and J.E. Dumont. 1989. Cell population kinetics in dog and human adult thyroid. *Clin Endocrinol (Oxf)* 31:655-665.

Dankort, D., E. Filenova, M. Collado, M. Serrano, K. Jones, and M. McMahon. 2007. A new mouse model to explore the initiation, progression, and therapy of BRAFV600E-induced lung tumors. *Genes Dev* 21:379-384.

de Biase, D., V. Cesari, M. Visani, G.P. Casadei, N. Cremonini, G. Gandolfi, V. Sancisi, M. Ragazzi, A. Pession, A. Ciarrocchi, and G. Tallini. 2014. High-sensitivity BRAF mutation analysis: BRAF V600E is acquired early during tumor development but is heterogeneously distributed in a subset of papillary thyroid carcinomas. *J Clin Endocrinol Metab* 99:E1530-1538.

Derwahl, M., and D. Nicula. 2014. Estrogen and its role in thyroid cancer. *Endocr Relat Cancer* 21:T273-283.

Dralle, H., A. Machens, J. Basa, V. Fatourechi, S. Franceschi, I.D. Hay, Y.E. Nikiforov, F. Pacini, J.L. Pasieka, and S.I. Sherman. 2015. Follicular cell-derived thyroid cancer. *Nat Rev Dis Primers* 1:15077.

Echeverria, G.V., E. Powell, S. Seth, Z. Ge, A. Carugo, C. Bristow, M. Peoples, F. Robinson, H. Qiu, J. Shao, S.L. Jeter-Jones, X. Zhang, V. Ramamoorthy, S. Cai, W. Wu, G. Draetta, S.L. Moulder, W.F. Symmans, J.T. Chang, T.P. Heffernan, and H. Piwnica-Worms. 2018. High-resolution clonal mapping of multi-organ metastasis in triple negative breast cancer. *Nat Commun* 9:5079.

Fernandez, L.P., A. Lopez-Marquez, and P. Santisteban. 2015. Thyroid transcription factors in development, differentiation and disease. *Nat Rev Endocrinol* 11:29-42.

Finkel, A., L. Liba, E. Simon, T. Bick, E. Prinz, E. Sabo, O. Ben-Izhak, and D. Hershkovitz. 2016. Subclonality for BRAF Mutation in Papillary Thyroid Carcinoma Is Associated With Earlier Disease Stage. *J Clin Endocrinol Metab* 101:1407-1413.

Franco, A.T., R. Malaguarnera, S. Refetoff, X.H. Liao, E. Lundsmith, S. Kimura, C. Pritchard, R. Marais, T.F. Davies, L.S. Weinstein, M. Chen, N. Rosen, R. Ghossein, J.A. Knauf, and J.A. Fagin. 2011. Thyrotrophin receptor signaling dependence of Braf-induced thyroid tumor initiation in mice. *Proc Natl Acad Sci U S A* 108:1615-1620.

Fugazzola, L., M. Muzza, G. Pogliaghi, and M. Vitale. 2020. Intratumoral Genetic Heterogeneity in Papillary Thyroid Cancer: Occurrence and Clinical Significance. *Cancers (Basel)* 12:

Garcia, S.B., M. Novelli, and N.A. Wright. 2000. The clonal origin and clonal evolution of epithelial tumours. *Int J Exp Pathol* 81:89-116.

Gawade, S., C. Mayer, K. Hafen, T. Barthlott, W. Krenger, and G. Szinnai. 2016. Cell Growth Dynamics in Embryonic and Adult Mouse Thyroid Revealed by a Novel Approach to Detect Thyroid Gland Subpopulations. *Thyroid* 26:591-599.

Ghossein, R.A., N. Katabi, and J.A. Fagin. 2013. Immunohistochemical detection of mutated BRAF V600E supports the clonal origin of BRAF-induced thyroid cancers along the spectrum of disease progression. *J Clin Endocrinol Metab* 98:E1414-1421.

Giannini, R., C. Ugolini, C. Lupi, A. Proietti, R. Elisei, G. Salvatore, P. Berti, G. Materazzi, P. Miccoli, M. Santoro, and F. Basolo. 2007. The heterogeneous distribution of BRAF mutation supports the independent clonal origin of distinct tumor foci in multifocal papillary thyroid carcinoma. *J Clin Endocrinol Metab* 92:3511-3516.

Gopal, R.K., K. Kubler, S.E. Calvo, P. Polak, D. Livitz, D. Rosebrock, P.M. Sadow, B. Campbell, S.E. Donovan, S. Amin, B.J. Gigliotti, Z. Grabarek, J.M. Hess, C. Stewart, L.Z. Braunstein, P.F. Arndt, S. Mordecai, A.R. Shih, F. Chaves, T. Zhan, C.C. Lubitz, J. Kim, A.J. Iafrate, L. Wirth, S. Parangi, I. Leshchiner, G.H. Daniels, V.K. Mootha, D. Dias-Santagata, G. Getz, and D.G. McFadden. 2018. Widespread Chromosomal Losses and Mitochondrial DNA Alterations as Genetic Drivers in Hurthle Cell Carcinoma. *Cancer Cell* 34:242-255 e245.

Halberg, R.B., and W.F. Dove. 2007. Polyclonal tumors in the mammalian intestine: are interactions among multiple initiated clones necessary for tumor initiation, growth, and progression? *Cell Cycle* 6:44-51.

Harach, H.R., K.O. Franssila, and V.M. Wasenius. 1985. Occult papillary carcinoma of the thyroid. A "normal" finding in Finland. A systematic autopsy study. *Cancer* 56:531-538.

Howell, G.M., S.P. Hodak, and L. Yip. 2013. RAS mutations in thyroid cancer. *Oncologist* 18:926-932.

Ingeson-Carlsson, C., and M. Nilsson. 2013. Switching from MAPK-dependent to MAPK-independent repression of the sodium-iodide symporter in 2D and 3D cultured normal thyroid cells. *Mol Cell Endocrinol* 381:241-254.

Jovanovic, L., B. Delahunt, B. McIver, N.L. Eberhardt, and S.K. Grebe. 2003. Thyroid gland clonality revisited: the embryonal patch size of the normal human thyroid gland is very large, suggesting X-chromosome inactivation tumor clonality studies of thyroid tumors have to be interpreted with caution. *J Clin Endocrinol Metab* 88:3284-3291.

Koboldt, D.C., K. Chen, T. Wylie, D.E. Larson, M.D. McLellan, E.R. Mardis, G.M. Weinstock, R.K. Wilson, and L. Ding. 2009. VarScan: variant detection in massively parallel sequencing of individual and pooled samples. *Bioinformatics* 25:2283-2285.

Kon, S., K. Ishibashi, H. Katoh, S. Kitamoto, T. Shirai, S. Tanaka, M. Kajita, S. Ishikawa, H. Yamauchi, Y. Yako, T. Kamasaki, T. Matsumoto, H. Watanabe, R. Egami, A. Sasaki, A. Nishikawa, I. Kameda, T. Maruyama, R. Narumi, T. Morita, Y. Sasaki, R. Enoki, S. Honma, H. Imamura, M. Oshima, T. Soga, J.I. Miyazaki, M.R. Duchen, J.M. Nam, Y. Onodera, S. Yoshioka, J. Kikuta, M. Ishii, M. Imajo, E. Nishida, Y. Fujioka, Y. Ohba, T. Sato, and Y. Fujita. 2017. Cell competition with normal epithelial cells promotes apical extrusion of transformed cells through metabolic changes. *Nat Cell Biol* 19:530-541.

Kopp, P., E.T. Kimura, S. Aeschimann, M. Oestreicher, A. Tobler, M.F. Fey, and H. Studer. 1994. Polyclonal and monoclonal thyroid nodules coexist within human multinodular goiters. *J Clin Endocrinol Metab* 79:134-139.

Landa, I., and J.A. Knauf. 2019. Mouse Models as a Tool for Understanding Progression in Braf(V600E)-Driven Thyroid Cancers. *Endocrinol Metab (Seoul)* 34:11-22.

Li, H., and R. Durbin. 2009. Fast and accurate short read alignment with Burrows-Wheeler transform. *Bioinformatics* 25:1754-1760.

Liang, S., E. Johansson, G. Barila, D.L. Altschuler, H. Fagman, and M. Nilsson. 2018. A branching morphogenesis program governs embryonic growth of the thyroid gland. *Development* 145:

Liu, J., S.G. Willet, E.D. Bankaitis, Y. Xu, C.V. Wright, and G. Gu. 2013. Non-parallel recombination limits Cre-LoxP-based reporters as precise indicators of conditional genetic manipulation. *Genesis* 51:436-442.

Lu, Z., J. Sheng, Y. Zhang, J. Deng, Y. Li, A. Lu, J. Zhang, H. Yu, M. Zhang, Z. Xiong, H. Yan, B.H. Diplas, Y. Lu, and B. Liu. 2016. Clonality analysis of multifocal papillary thyroid carcinoma by using genetic profiles. *J Pathol* 239:72-83.

Ma, D.F., K. Sudo, H. Tezuka, T. Kondo, T. Nakazawa, D.F. Niu, T. Kawasaki, K. Mochizuki, T. Yamane, and R. Katoh. 2010. Polyclonal origin of hormone-producing cell populations evaluated as a direct in situ demonstration in EGFP/BALB/C chimeric mice. *J Endocrinol* 207:17-25.

Manley, N.R., and M.R. Capecchi. 1995. The role of Hoxa-3 in mouse thymus and thyroid development. *Development* 121:1989-2003.

McKenna, A., M. Hanna, E. Banks, A. Sivachenko, K. Cibulskis, A. Kernytsky, K. Garimella, D. Altshuler, S. Gabriel, M. Daly, and M.A. DePristo. 2010. The Genome Analysis Toolkit: a MapReduce framework for analyzing next-generation DNA sequencing data. *Genome Res* 20:1297-1303.

Mitsutake, N., T. Fukushima, M. Matsuse, T. Rogounovitch, V. Saenko, S. Uchino, M. Ito, K. Suzuki, S. Suzuki, and S. Yamashita. 2015. BRAF(V600E) mutation is highly prevalent in thyroid carcinomas in the young population in Fukushima: a different oncogenic profile from Chernobyl. *Sci Rep* 5:16976.

Mizutani, K., M. Onda, S. Asaka, J. Akaishi, S. Miyamoto, A. Yoshida, M. Nagahama, K. Ito, and M. Emi. 2005. Overexpressed in anaplastic thyroid carcinoma-1 (OEATC-1) as a novel gene responsible for anaplastic thyroid carcinoma. *Cancer* 103:1785-1790.

Muzumdar, M.D., B. Tasic, K. Miyamichi, L. Li, and L. Luo. 2007. A global double-fluorescent Cre reporter mouse. *Genesis* 45:593-605.

Nilsson, M., and H. Fagman. 2013. Mechanisms of Thyroid Development and Dysgenesis: An Analysis Based on Developmental Stages and Concurrent Embryonic Anatomy. *Curr Top Dev Biol* 106:123-170.

Nilsson, M., and H. Fagman. 2017. Development of the thyroid gland. *Development* 144:2123-2140.

Novelli, M., A. Cossu, D. Oukrif, A. Quaglia, S. Lakhani, R. Poulsom, P. Sasieni, P. Carta, M. Contini, A. Pasca, G. Palmieri, W. Bodmer, F. Tanda, and N. Wright. 2003. X-inactivation patch size in human female tissue confounds the assessment of tumor clonality. *Proc Natl Acad Sci U S A* 100:3311-3314.

Parsons, B.L. 2018. Multiclonal tumor origin: Evidence and implications. *Mutat Res* 777:1-18.

Peter, H.J., H. Gerber, H. Studer, and S. Smeds. 1985. Pathogenesis of heterogeneity in human multinodular goiter. A study on growth and function of thyroid tissue transplanted onto nude mice. *J Clin Invest* 76:1992-2002.

Pratilas, C.A., B.S. Taylor, Q. Ye, A. Viale, C. Sander, D.B. Solit, and N. Rosen. 2009. (V600E)BRAF is associated with disabled feedback inhibition of RAF-MEK signaling and elevated transcriptional output of the pathway. *Proc Natl Acad Sci U S A* 106:4519-4524.

Rahbari, R., L. Zhang, and E. Kebebew. 2010. Thyroid cancer gender disparity. *Future Oncol* 6:1771-1779.

Reeves, M.Q., E. Kandyba, S. Harris, R. Del Rosario, and A. Balmain. 2018. Multicolour lineage tracing reveals clonal dynamics of squamous carcinoma evolution from initiation to metastasis. *Nat Cell Biol* 20:699-709.

Ricarte-Filho, J.C., M. Ryder, D.A. Chitale, M. Rivera, A. Heguy, M. Ladanyi, M. Janakiraman, D. Solit, J.A. Knauf, R.M. Tuttle, R.A. Ghossein, and J.A. Fagin. 2009. Mutational profile of advanced primary and metastatic radioactive iodine-refractory thyroid cancers reveals distinct pathogenetic roles for BRAF, PIK3CA, and AKT1. *Cancer Res* 69:4885-4893.

Saad, A.G., S. Kumar, E. Ron, J.H. Lubin, J. Stanek, K.E. Bove, and Y.E. Nikiforov. 2006. Proliferative activity of human thyroid cells in various age groups and its correlation with the risk of thyroid cancer after radiation exposure. *J Clin Endocrinol Metab* 91:2672-2677.

Sellitti, D.F., and K. Suzuki. 2014. Intrinsic regulation of thyroid function by thyroglobulin. *Thyroid* 24:625-638.

Shabana, W., F. Delange, M. Freson, M. Osteaux, and J. De Schepper. 2000. Prevalence of thyroid hemiagenesis: ultrasound screening in normal children. *Eur J Pediatr* 159:456-458.

Shattuck, T.M., W.H. Westra, P.W. Ladenson, and A. Arnold. 2005. Independent clonal origins of distinct tumor foci in multifocal papillary thyroid carcinoma. *N Engl J Med* 352:2406-2412.

Shimamura, M., M. Nakahara, F. Orim, T. Kurashige, N. Mitsutake, M. Nakashima, S. Kondo, M. Yamada, R. Taguchi, S. Kimura, and Y. Nagayama. 2013. Postnatal expression of BRAFV600E does not induce thyroid cancer in mouse models of thyroid papillary carcinoma. *Endocrinology* 154:4423-4430.

Shimamura, M., N. Shibusawa, T. Kurashige, Z. Mussazhanova, H. Matsuzaki, M. Nakashima, M. Yamada, and Y. Nagayama. 2018. Mouse models of sporadic thyroid cancer derived from BRAFV600E alone or in combination with PTEN haploinsufficiency under physiologic TSH levels. *PLoS One* 13:e0201365.

Smeds, S., H.J. Peter, E. Jortso, H. Gerber, and H. Studer. 1987. Naturally occurring clones of cells with high intrinsic proliferation potential within the follicular epithelium of mouse thyroids. *Cancer Res* 47:1646-1651.

Soriano, P. 1999. Generalized lacZ expression with the ROSA26 Cre reporter strain. *Nat Genet* 21:70-71.

Studer, H., R. Forster, A. Conti, H. Kohler, A. Haeberli, and H. Engler. 1978. Transformation of normal follicles into thyrotropin-refractory "cold" follicles in the aging mouse thyroid gland. *Endocrinology* 102:1576-1586.

Studer, H., H.J. Peter, and H. Gerber. 1989. Natural heterogeneity of thyroid cells: the basis for understanding thyroid function and nodular goiter growth. *Endocr Rev* 10:125-135.

Swanton, C. 2012. Intratumor heterogeneity: evolution through space and time. *Cancer Res* 72:4875-4882.

Thliveris, A.T., B. Schwefel, L. Clipson, L. Plesh, C.D. Zahm, A.A. Leystra, M.K. Washington, R. Sullivan, D.A. Deming, M.A. Newton, and R.B. Halberg. 2013. Transformation of epithelial cells through recruitment leads to polyclonal intestinal tumors. *Proc Natl Acad Sci U S A* 110:11523-11528.

Thomas, G.A., D. Williams, and E.D. Williams. 1989. The clonal origin of thyroid nodules and adenomas. *Am J Pathol* 134:141-147.

Turajlic, S., A. Sottoriva, T. Graham, and C. Swanton. 2019. Resolving genetic heterogeneity in cancer. *Nat Rev Genet* 20:404-416.

Undeutsch, H., C. Lof, S. Offermanns, and J. Kero. 2014. A mouse model with tamoxifen-inducible thyrocyte-specific cre recombinase activity. *Genesis* 52:333-340.

van der Heijden, M., D.M. Miedema, B. Waclaw, V.L. Veenstra, M.C. Lecca, L.E. Nijman, E. van Dijk, S.M. van Neerven, S.C. Lodestijn, K.J. Lenos, N.E. de Groot, P.R. Prasetyanti, A. Arricibita Varea, D.J. Winton, J.P. Medema, E. Morrissey, B. Ylstra, M.A. Nowak, M.F. Bijlsma, and L. Vermeulen. 2019. Spatiotemporal regulation of clonogenicity in colorectal cancer xenografts. *Proc Natl Acad Sci U S A* 116:6140-6145.

van Isselt, J.W., J.M. de Klerk, P.P. van Rijk, A.P. van Gils, L.J. Polman, C. Kamphuis, R. Meijer, and F.J. Beekman. 2003. Comparison of methods for thyroid volume estimation in patients with Graves' disease. *Eur J Nucl Med Mol Imaging* 30:525-531.

Wang, K., M. Li, and H. Hakonarson. 2010. ANNOVAR: functional annotation of genetic variants from high-throughput sequencing data. *Nucleic Acids Res* 38:e164.

Vermeulen, L., E. Morrissey, M. van der Heijden, A.M. Nicholson, A. Sottoriva, S. Buczacki, R. Kemp, S. Tavare, and D.J. Winton. 2013. Defining stem cell dynamics in models of intestinal tumor initiation. *Science* 342:995-998.

Villacorte, M., A.S. Delmarcelle, M. Lernoux, M. Bouquet, P. Lemoine, J. Bolsee, L. Umans, S.C. de Sousa Lopes, P. Van Der Smissen, T. Sasaki, G. Bommer, P. Henriet, S. Refetoff, F.P. Lemaigre, A. Zwijsen, P.J. Courtoy, and C.E. Pierreux. 2016. Thyroid follicle development requires Smad1/5- and endothelial cell-dependent basement membrane assembly. *Development* 143:1958-1970.

Williams, D. 2008. Radiation carcinogenesis: lessons from Chernobyl. *Oncogene* 27 Suppl 2:S9-18.

Williams, D. 2015. Thyroid Growth and Cancer. *Eur Thyroid J* 4:164-173.

Xing, M. 2005. BRAF mutation in thyroid cancer. *Endocr Relat Cancer* 12:245-262.

Yamashita, S., and S. Suzuki. 2013. Risk of thyroid cancer after the Fukushima nuclear power plant accident. *Respir Investig* 51:128-133.

Ye, J., G. Coulouris, I. Zaretskaya, I. Cutcutache, S. Rozen, and T.L. Madden. 2012. Primer-BLAST: a tool to design target-specific primers for polymerase chain reaction. *BMC Bioinformatics* 13:134.

Yeager, N., A. Klein-Szanto, S. Kimura, and A. Di Cristofano. 2007. Pten loss in the mouse thyroid causes goiter and follicular adenomas: insights into thyroid function and Cowden disease pathogenesis. *Cancer Res* 67:959-966.

Zou, M., E.Y. Baitei, R.A. Al-Rijjal, R.S. Parhar, F.A. Al-Mohanna, S. Kimura, C. Pritchard, H.A. Binessa, A.S. Alzahrani, H.H. Al-Khalaf, A. Hawwari, M. Akhtar, A.M. Assiri, B.F. Meyer, and Y. Shi. 2016. TSH overcomes Braf(V600E)-induced senescence to promote tumor progression via downregulation of p53 expression in papillary thyroid cancer. *Oncogene* 35:1909-1918.

Figures

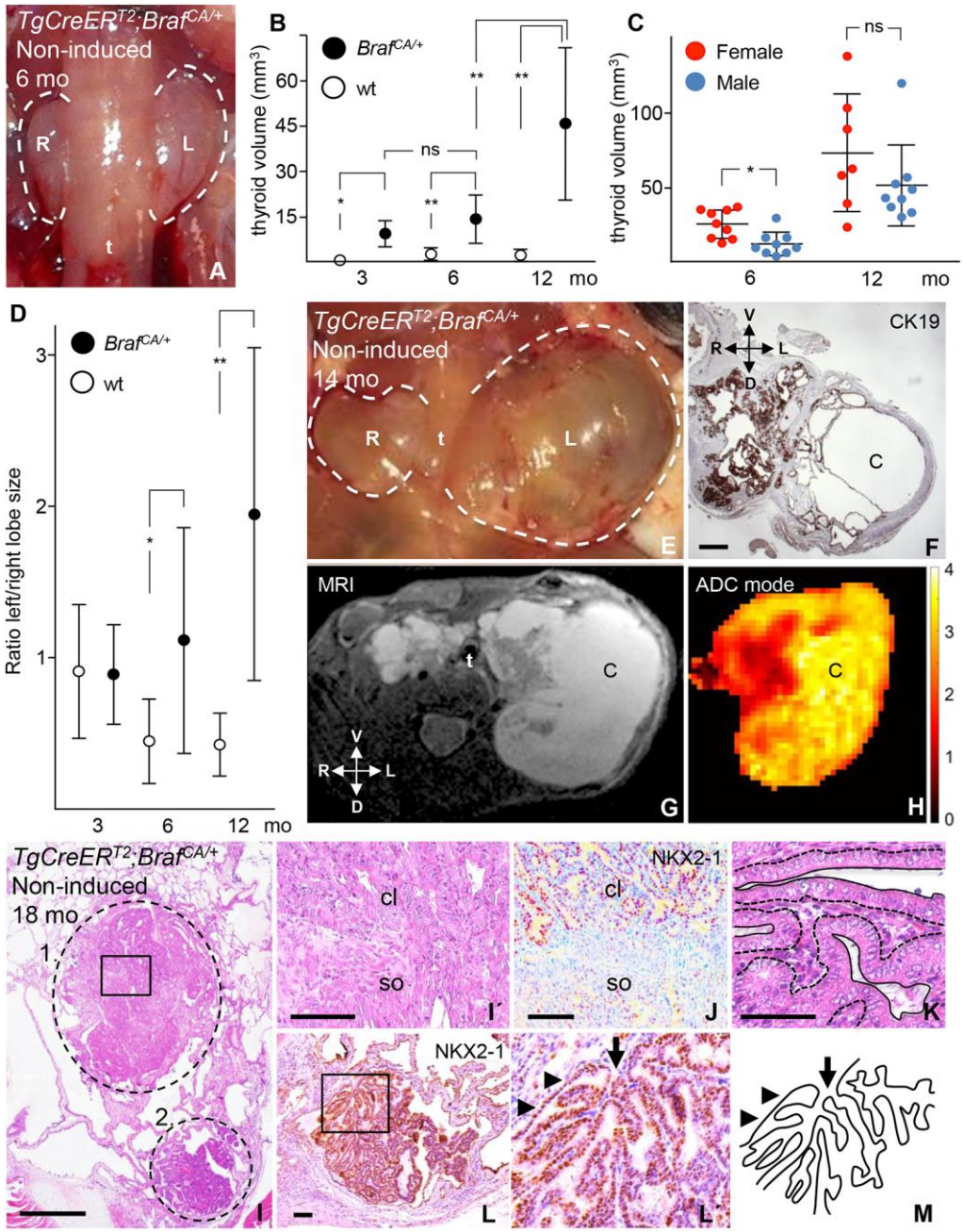

Fig. 1. Occurrence of papillary thyroid carcinoma (PTC) in non-induced *TgCreER^{T2};Braf$^{CA/+}$* mice devoid of tamoxifen injections. Data from 3-18 months (mo) old wildtype (wt) and *Braf^{CA}* mutants. Thyroid volumes estimated from lobe diameter measurements. **A-E**, Thyroid

enlargement. **A, E**, Frontal view, *in situ* micrographs. **B**, Time-dependence. **C**, Sex-dependence. **D, E**, Asymmetric lobe growth. Mean±sd (*, $p<0.005$; **, $p<0.0001$); animal numbers (n) at 3 mo: wt (12), mutants (17); at 6 mo: wt (16), mutants (20); at 12 mo: wt (12), mutants (18), or as indicated. **F**, $CK19^+$ expression (IHC staining). **G, H**, T2-weighted MRI (G; same specimen as in E and F; for entire stack series, see Video 1) and ADC map (H) of the same image. Color bar indicates solid (red) and cystic (yellow) tumors based on apparent diffusion coefficient ($\mu m^2/ms$). "C" in F-H indicates corresponding cystic tumor portions. Used technology delimited resolution of images. **I-L**, Inter- and intratumor heterogeneity of multifocal PTCs (encircled; HE staining. Additional tumors present in the same thyroid specimen are imaged in Figs. S1 and S2). **I**, Overview of two adjacent tumor foci (1 and 2); I´, high power of boxed area in I, indicating transition of tumor growth pattern. **J,** NKX2-1 expression (IHC); parallel section to L´ image. **K**, Nuclear characteristics of tumor cells; detail of PTC tumor 1 in I. Interface towards lumen and stroma of tumor tissue is outlined. **L**, NKX2-1 expression in PTC tumor 2 in I. L´, high power of boxed area in L. **M**, Cartoon outlining papillary growth of tumor in L´. Anatomical orientation: R, right; L, left; V, ventral; D; dorsal. t, trachea; cl, classical variant of PTC; so, solid variant of PTC; arrows, tumor stalk; arrowheads, follicular wall enclosing tumor. Scale bars: 500 (F, I) and 100 (I´, F, K) µm.

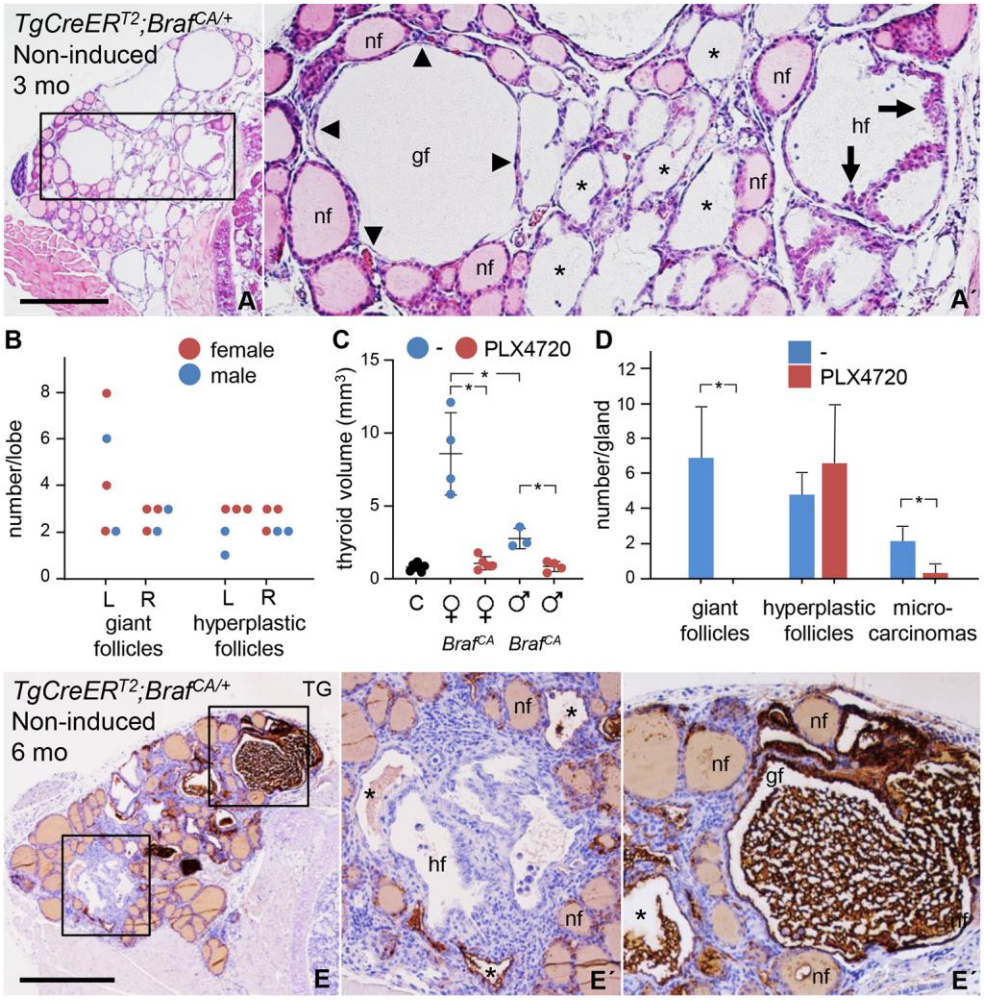

Fig. 2. Early stages of thyroid tumor development following spontaneous *Braf*^{CA} activation. **A**, Heterotypic follicular abnormalities at 3 months (mo); A´, boxed area in A (HE staining). Asterisks indicate appearance of follicles with translucent interior i.e. lacking colloid. **B-D**, Quantitative changes and responsiveness to vemurafenib. Dietary PLX4720 (417 ppm) was supplied daily from 4 weeks until sacrifice at 3 mo; data obtained at 3 mo based on serial sections. **B**, Number of neoplastic follicles in untreated mutants (individual data). **C**, Inhibition of thyroid enlargement (individual data; mean±sd; *, p<0.005). **D**, Heterogeneous drug response of neoplastic lesions; mean±sd (*, p<0.005) of (n): wt (5); untreated mutants (7), drug-treated

mutants (9). **E**, Early loss of thyroglobulin (TG) expression in neoplastic lesions (IHC). Representative thyroid images from a 6 mo old mutant. E´, boxed areas in E. L, left lobe; R, right lobe; nf, normal follicle; hf, hyperplastic follicle; gf, giant follicle; mic, microcarcinoma; ; arrows, hyperplastic epithelium; arrowheads, flat epithelium; C, control = wildtype (wt). Scale bars: 500 (A, E) µm.

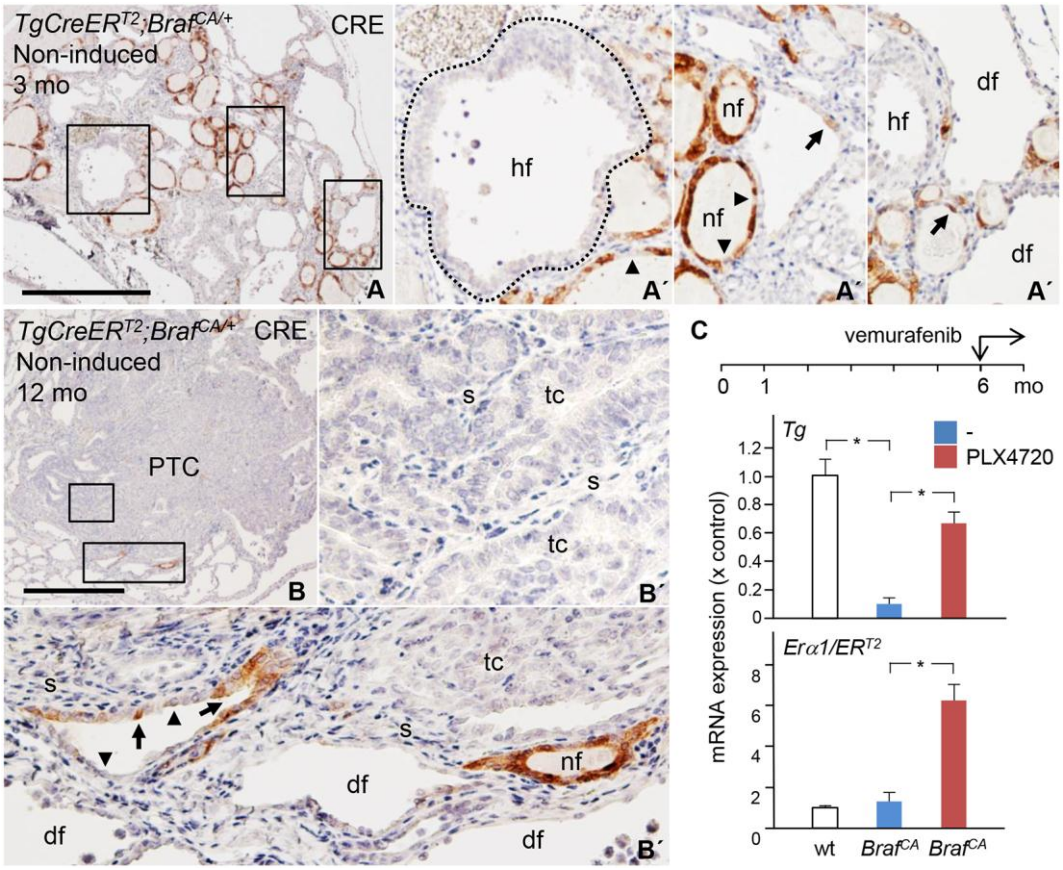

Fig. 3. Diminished *Cre* driver expression in BRAF-mutant mouse thyroid cells. Data obtained from 3-12 months (mo) old *TgCreER*^{T2}*;Braf*$^{CA/+}$ mice devoid of tamoxifen treatment. **A, B,** Tissue distribution of CRE positive and negative cells (IHC staining). A´ and B´ show boxed areas in A and B, respectively. C Recovery of *TgCreERT2* expression by vemurafenib (qPCR data); drug treatment started at 6 mo and lasted for 1 mo. nf, normal follicles; hf, hyperplastic follicles (encircled in A´); df, dilated follicles; PTC, papillary thyroid carcinoma; tc, tumor cells; s, stroma; arrows, CRE^{+} cells; arrowheads, CRE negative cells. Scale bars: 500 (A, B) µm.

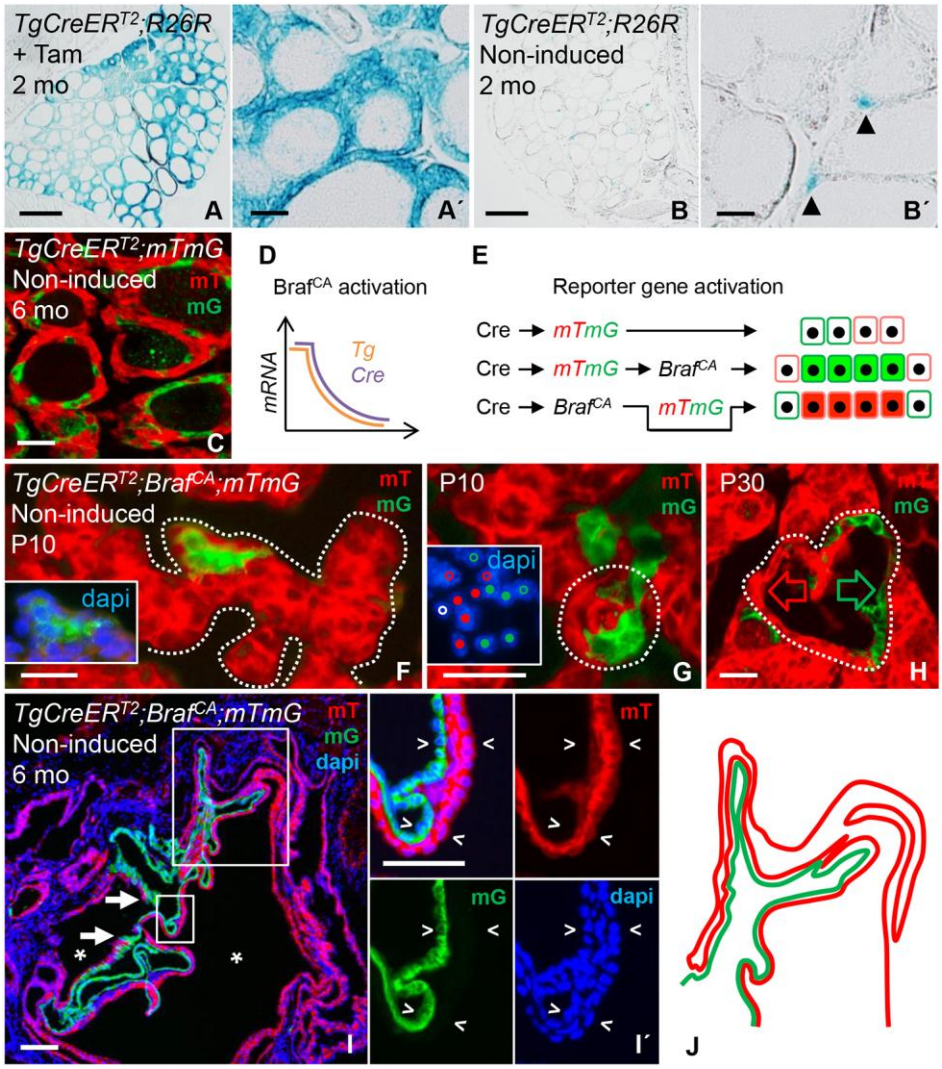

Fig. 4. Clonal tracing of mutant thyroid cells after spontaneous *Braf*^{CA} activation. **A, B**, Comparison of *Rosa26* reporter activation in induced (A) and non-induced (B) *TgCreER*^{T2}*;R26R* mice (X-gal staining); A´ and B´ show labeled cells at high resolution (arrowheads in B´). **C**, Distribution of normal cells subjected to spontaneous *mTmG* activation by leaky CRE. **D, E**, Expected outcomes of tracing progeny of BRAF-mutant cells depending on down-regulation of the *Cre* driver (D) and whether *mTmG* is activated before or after *Braf*^{CA} (E). **F-H**, Clonal expansion accompanying folliculogenesis in *TgCreER*^{T2}*;Braf* $^{CA/+}$*;mTmG* mice at postnatal days 10 (P10) and 30 (P30); representative thyroid images from serial sections. **F**, Pre-follicular

branching parenchyma (outlined); inset indicate dapi-stained nuclei of mG^+ clone. **G**, Nascent oligoclonal follicle (encircled); inset indicates dapi-stained nuclei corresponding to mG^+ and mT^+ follicular cells (filled dots) and surrounding cells (open dots) including a stromal cell (white dot). **H**, Hyperplastic oligoclonal follicle (encircled); for a comprehensive imaging of contiguous mG^+ and mT^+ epithelial domains (open arrows), see stack series in Fig. S5. **I**, Oligoclonal microcarcinoma involving clonal cooperativity of papillary growth. I´ show single and combined fluorescence channels of small boxed area in I; brackets demarcate planar expansion of adjacent mG^+ and mT^+ clones. Asterisks, lumen of neoplasm; arrows, transition zone of mT^+ and mG^+ epithelial domains. **J**, Cartoon of large boxed are in I indicating lamellar pattern of oligoclonal growth. Scale bars: 500 (A, B), 100 (A´, B´, C, I) and 25 (F-H) µm.

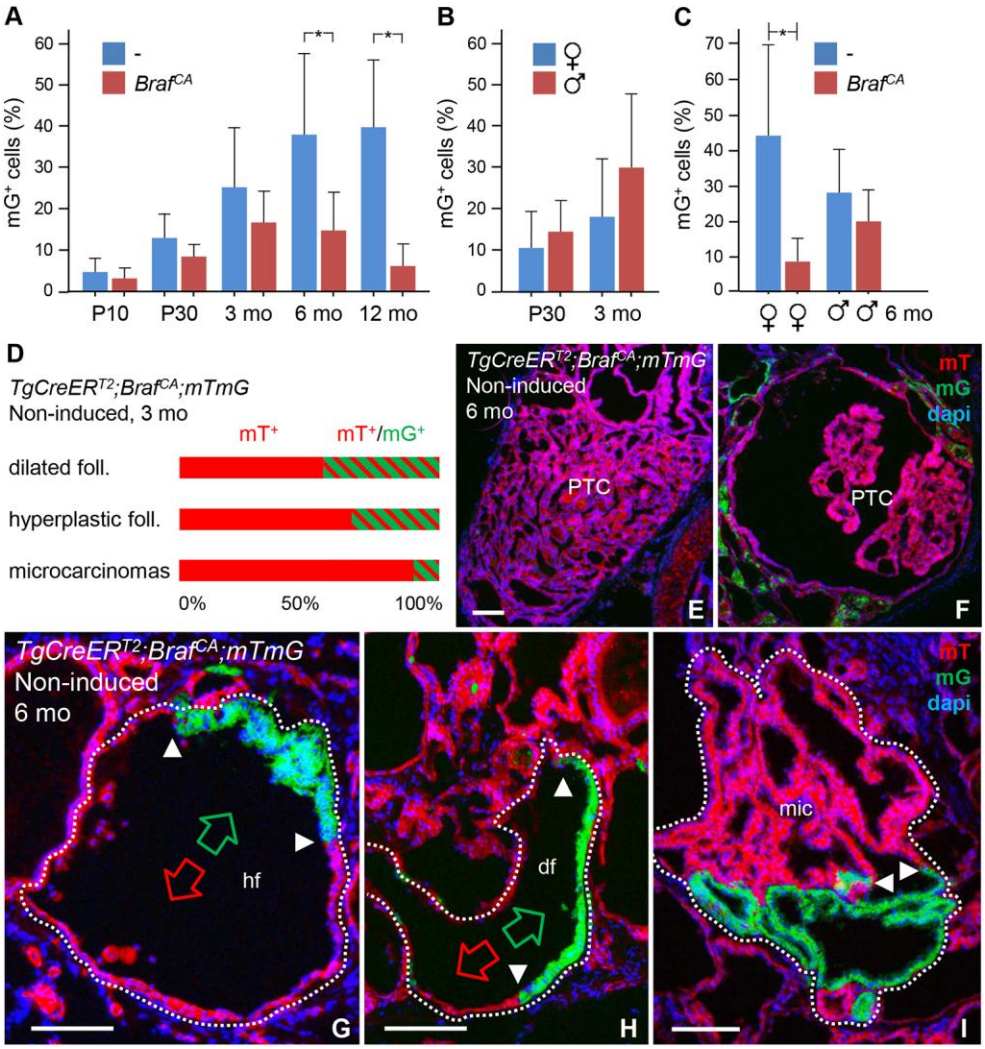

Fig. 5. Clonal selection during tumorigenesis in *TgCreER^{T2};Braf$^{CA/+}$;mTmG* mice. **A-C**, Clonal growth as estimated by counting mG$^+$ thyroid cells in serial sections (three levels/lobe) of mutant mice from P10 to 12 months (mo) of age in comparison to incidence of spontaneous reporter gene activation in age-matched *TgCreER^{T2};mTmG* mice (controls). The percentage of mG$^+$ cells relates to the total number of dapi-stained cells excluding any stromal cells. **A**, Time-dependent accumulation of mG$^+$ cells; mean±sd (*, $p<0.005$; n=6 for each group and time point). **B**, Equal rates of reporter gene activation in male and female controls. **C**, Gender bias of clonal expansion of T$^+$ cells in mutants; mean±sd (*, $p<0.005$; n=3 for each group in B and C). **D**, Proportion of

mT^+ and compound mT^+/mG^+ lesions at 3 mo; mean values based on five serially sectioned thyroids (lesions composed of only mG^+ cells did not occur). **E, F**, Representative images of carcinomas consisting solely of mT^+ cells. **G-I**, Dual-labeled lesions (encircled) with distinct or indistinguishable growth pattern, respectively, of clones; arrowheads indicate clone borders. hf, hyperplastic follicle; df, dilated follicle; mic, microcarcinoma; PTC, papillary thyroid carcinoma. Scale bars: 100 µm.

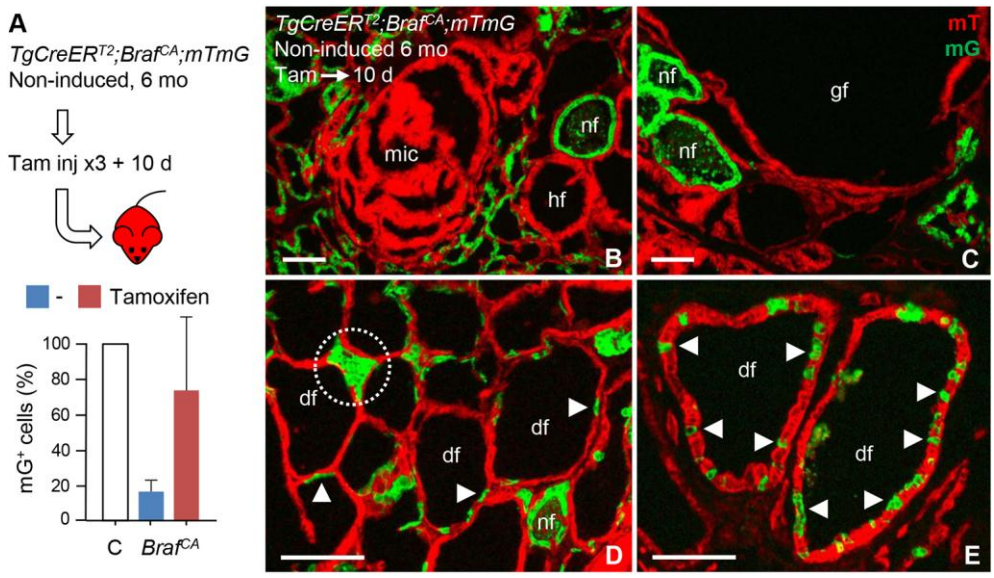

Fig. 6. Follicular distribution of BRAF-mutant cells. Six months (mo) old *TgCreER^{T2};Braf$^{CA/+}$;mTmG* mice were repeatedly injected with tamoxifen to distinguish unlabeled mutant cells from non-mutant cells with preserved CRE activity, and analyzed 10 days (d) thereafter. **A**, Induced reporter gene activation. Control (C) set to 100% corresponds to level of mTmG activation in age-matched *TgCreER^{T2};mTmG* mice. Mean±sd (n): controls (6), untreated mutants (3), tamoxifen-treated mutants (7); three section levels/gland. **B-E**, Density of induced cells in follicles of various size and shape. Arrowheads, responding mG^{+} cells; nf, normal follicle; hf, hyperplastic follicle; df, dilated follicle; gf, giant follicle; mic, microcarcinoma. Scale bars: 100 µm.

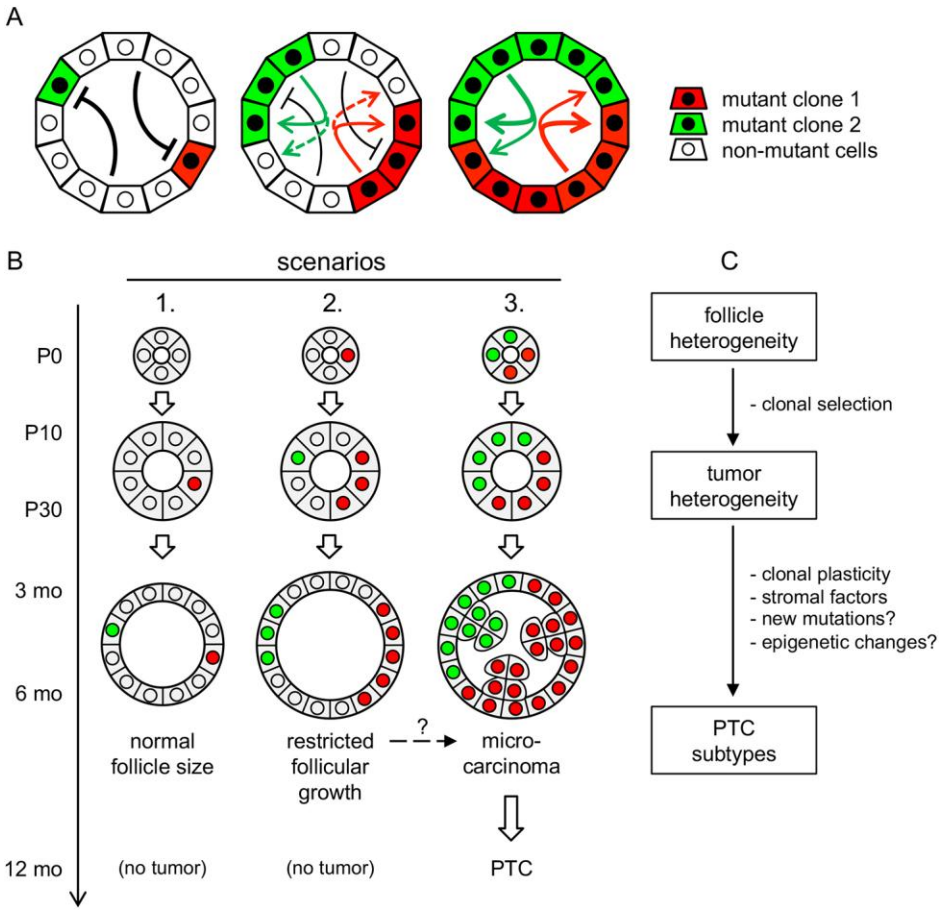

Fig. 7. Clonal evolution of tumor development and heterogeneity in sporadic thyroid cancer, as proposed from the present mouse model. **A**, Constraints on tumor initiation depending on cell composition of thyroid follicles. Variants correspond to tumor development scenarios outlined in B. Red and green arrows indicate suggested clonal cooperativity of mutant clones (solid lines) and putative bystander inhibitory effects of oncogenic activation on non-mutant cells (dashed lines). **B**, Tumor development promoted by follicle immaturity. Scenarios (1-3) based on timing and coincidence of independent oncogenic mutations (red and green). **C**, Spatial factors influencing tumor phenotype. See Discussion for further comments.

Table 1. Whole exome sequencing of thyroid carcinomas generated by spontaneous activation of *Braf*^{CA} in *TgCreER*^{T2};*Braf*$^{CA/+}$ mice.

Sex/age	Gene	Reference transcript	Mutation[3]	MAF
F/4[1]	-	-	ne	-
F/4[2]	-	-	ne	-
F/6[2]	*Syn1*	NM 013680	c.T25G/p.S9A	0.11
	Pclaf	NM026515	c.G143A/p.G48E	0.071
M/8[2]	*Chd5*	NM 029216	c.A5609C/p.D1870A	0.13
M/12[2]	*Cdhr2*	NM 001033364	c.C1543T/p.P515S	0.053
	Plk4	NM 173169	c.G2586T/p.O862H	0.14
	Spata31d1d	NM 177711	c.G431T/p.C144F	0.11

MAF, mutation allele fraction

[1]induced by tamoxifen

[2]non-induced (no tamoxifen)

[3]validated by sequencing

ne, not encountered

Table S1. Quality data from whole exome sequencing of thyroid carcinomas generated by spontaneous activation of *Braf*^{V600E} in *TgCreER*^{T2}*;Braf*$^{CA/+}$ mice.

Mouse Id	Sample[1]	Total number of reads	Mapped number of reads	% of mapped reads	Mean coverage
3182	Tumor	60027679	59294617	98.78	185.36
	Normal	28873205	28555696	98.91	90.0824
4187	Tumor	57690485	57690485	98.96	173.888
	Normal	43839295	43360247	98.91	135.016
4655	Tumor	85800968	84806007	98.85	260.843
	Normal	29903775	29544091	98.8	92.7111
4743	Tumor	71108114	69976003	98.41	209.029
	Normal	23167811	22835561	98.57	69.0573
4747	Tumor	73639412	72888030	98.98	223.971
	Normal	18999407	18809921	99.01	58.0215

[1]Normal refers to constitutional control tissues (kidney) obtained from the same mice

Table S2. Gene expression changes associated with dedifferentiation of Braf mutant thyroid cells after spontaneous and induced *Braf*^{CA} activation in *TgCreER*^{T2}*;Braf*$^{CA/+}$ mice.

	qPCR[1]				
Tam[2]	*Pax8*	*Tg*	*Slc5a5/Nis*	*Tpo*	*Tshr*
-	0,90 ± 0,19	0,57 ± 0,20	0,16 ± 0,03	0,45 ± 0,06	0,63 ± 0,11
+	0,25 ± 0,02	0,03 ± 0,01	0,15 ± 0,06	0,13 ± 0,04	0,19 ± 0,03

[1]Analysis of thyroid tissue samples obtained from 5 weeks + 10 days (± post-injection) old mice (n=3/group)
[2]Tamoxifen; i.p. injections daily x3 after weaning
[3]Mean ± sd; expression relative to transcript levels in control (*TgCreER*^{T2}) mice set to "1"

Movie 1. Magnetic resonance imaging (MRI) of multicentric papillary thyroid carcinomas. Scrolling stack of images based on transverse MRI encompassing the entire thyroid gland and surrounding neck tissues in a 14 month old *TgCreER*^{T2}*;Braf*$^{CA/+}$ mouse subjected to spontaneous (non-induced) *Braf*^{CA} activation. For technical data and keys to image details, see Materials & Methods and accompanying Figs. 1G and H. Image resolution is inherited to technical constraints.

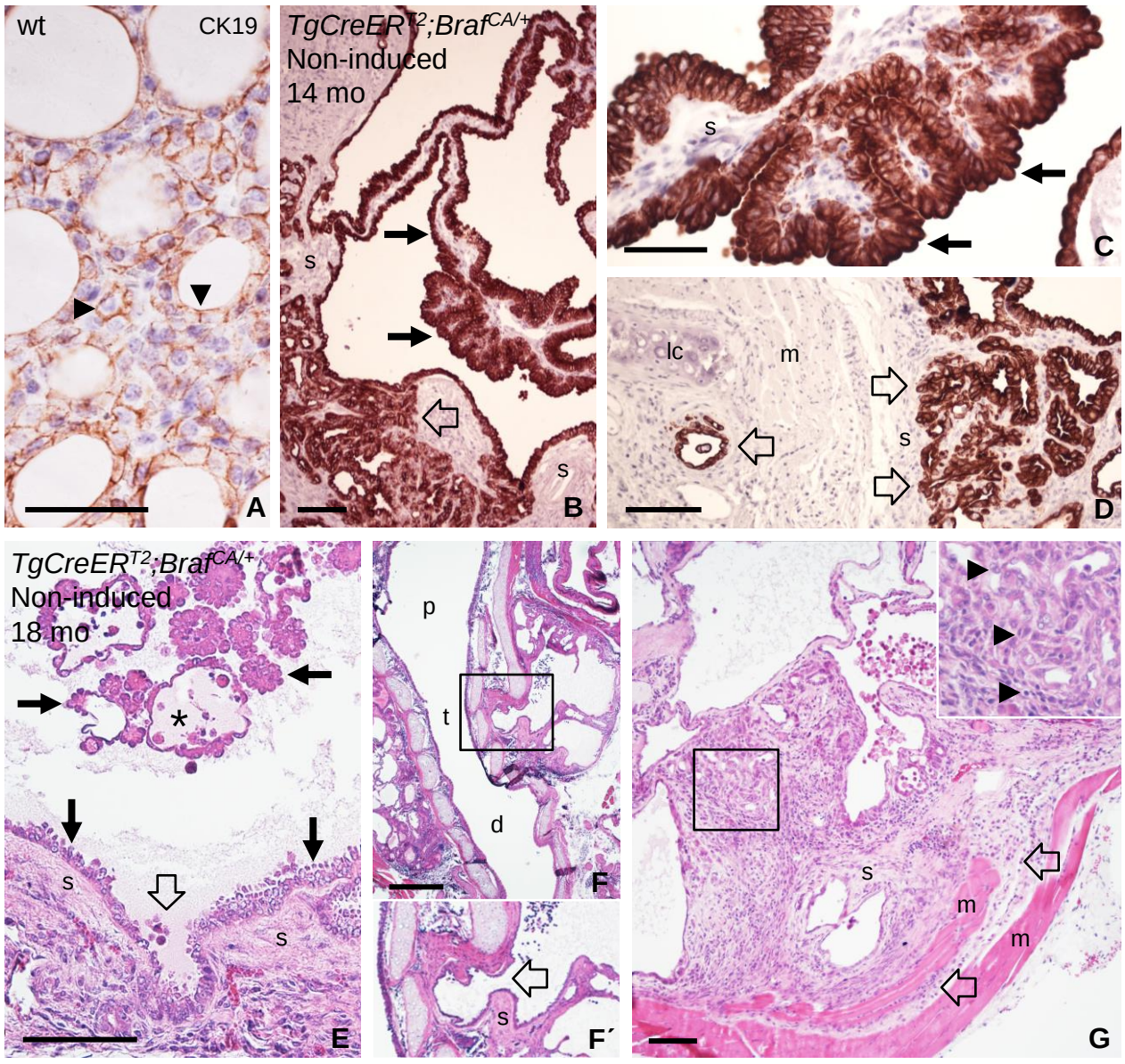

Fig. S1. Spontaneous *Braf*^{CA} activation generates CK19 positive papillary thyroid carcinoma (PTC) with signs of tumor invasiveness. Images obtained from 14 and 18 months (mo) old *TgCreER*^{T2}*;Braf*$^{CA/+}$ mice. CK19 immunohistochemistry (A-D). **A**, Weak CK19 expression in normal mouse thyroid. Arrowheads indicate preferential membranous localization of CK19 in follicular epithelial cells. **BC**, Strong expression of CK19 in tumor cells of a multilocular PTC. Arrows indicate tumorous epithelium lining enlarged follicular lumens and forming typical papillae. **D**, Stromal and extrathyroidal invasiveness of CK19^{+} thyroid tumor cells indicated by open arrows (also shown in B). B´ shows high power of boxed area in B. Note stromal infiltration of tumor cells (arrows). **E**, Cystic PTC with capsular invasion (open arrow). Note tumor cells display nuclear features typical of PTC and cell shape reminiscent of a hobnail-like phenotype. Asterisk indicates internal cavity of papillary formations projecting into the cyst. **F**, Cystic tumor infiltrating the trachea (open arrow in F´ = high power of boxed area in F). **G**, Solid tumor originating from the wall of an enlarged follicle. Inset shows detail of boxed area with heterotypic tumor cells and tumor-infiltrating lymphocytes indicated by arrowheads. Open arrows indicate extrathyroidal tumor invasion. s, stroma; m, skeletal muscle, lc, laryngeal cartilage; t, trachea; p, proximal; d, distal. Scale bars: 500 (F), 100 (B, D, E, G) and 50 (A, C) µm.

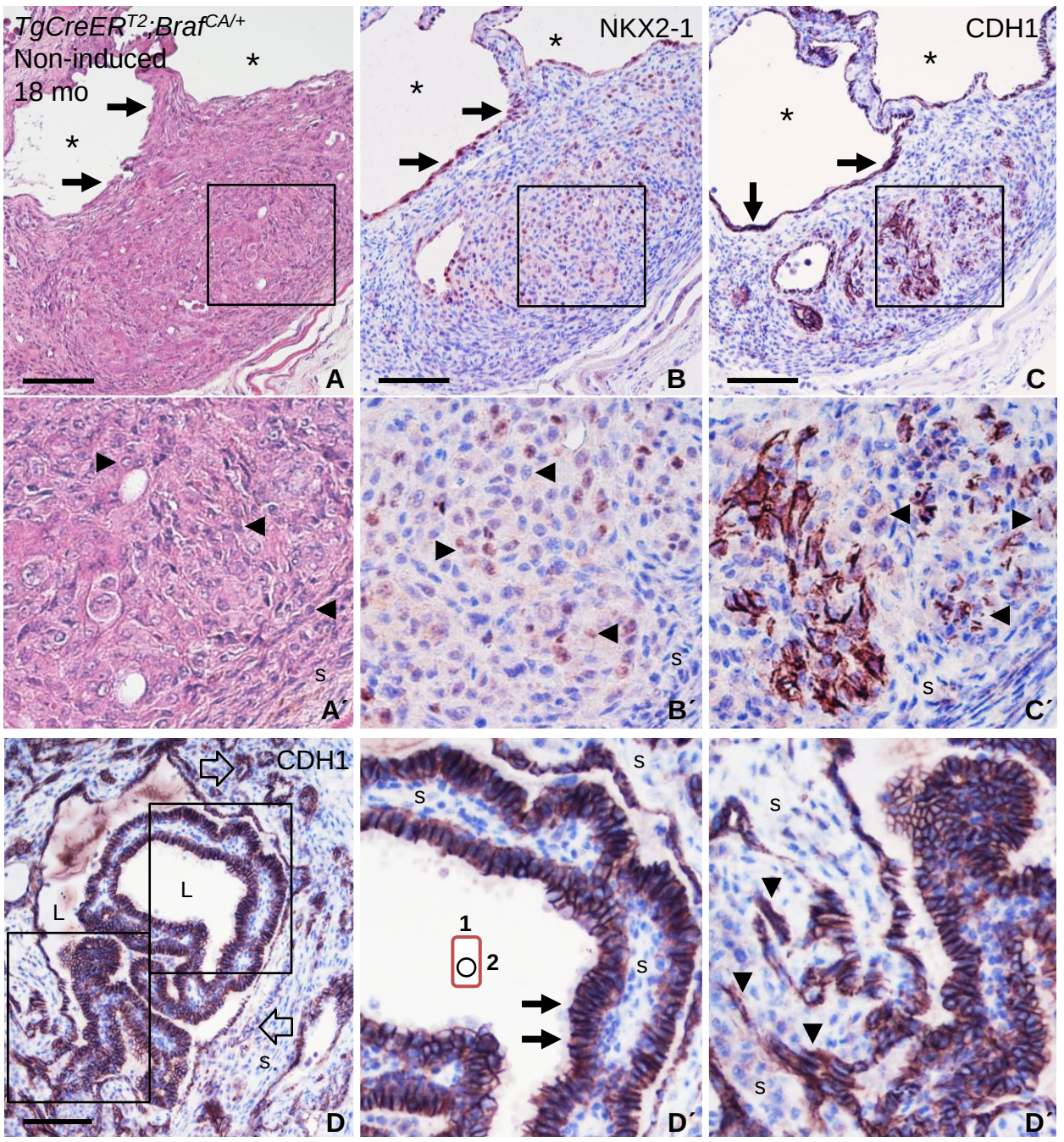

Fig. S2. Phenotype of tumor variants of papillary thyroid carcinoma (PTC) present in an 18 months old non-induced *TgCreER^{T2};Braf$^{CA/+}$* mouse. Figs. 1I-K and S1E-G derive from the same thyroid specimen. **A-C**, Solid variant of PTC adjacent to an enlarged, septate follicle (asterisks). Histology (A) and immunostaining for NKX2-1 (B) and E-cadherin (CDH1; C) on parallel sections. A´-C´ show high power of boxed areas. Arrows indicate flat epithelium strongly positive for both markers. Arrowheads show tumor cells with pleomorphic nuclei (A´), diminished expression of NKX2-1 (B´) and partial loss of CDH1 at cell contacts (C´). **D**, Tall-cell variant of PTC surrounded by abundant fibrous tissue intermixed with neoplastic follicles (large arrows). D´ highlights (left) predominant cell shape with length/width ratio 2:1 or more (arrows and cartoon) in central tumor and (right) signs of stromal invasion of CDH1+ tumor cells (arrowheads). L, lumen of tumor; s, stroma. Scale bars (A-D): 100 µm.

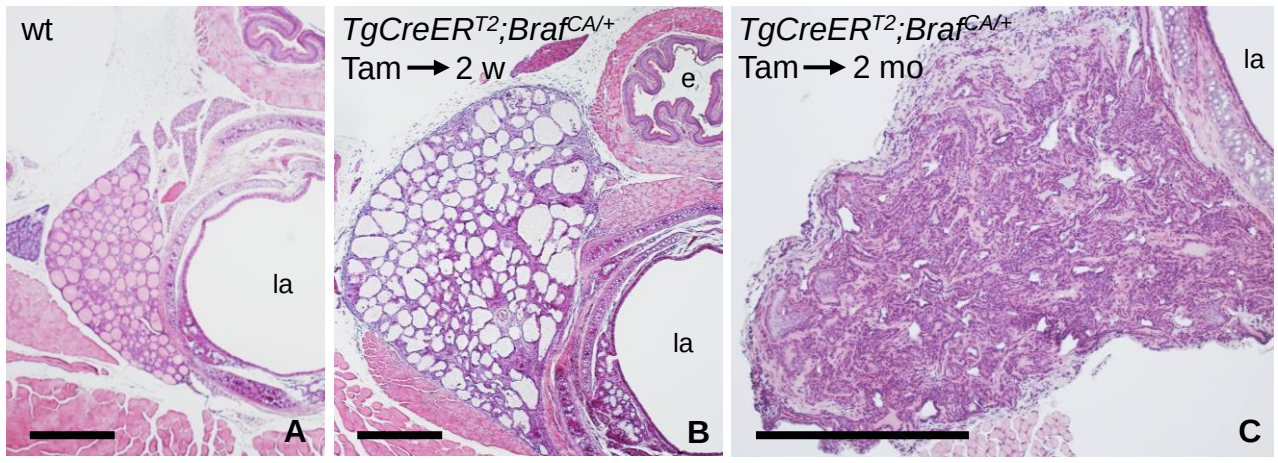

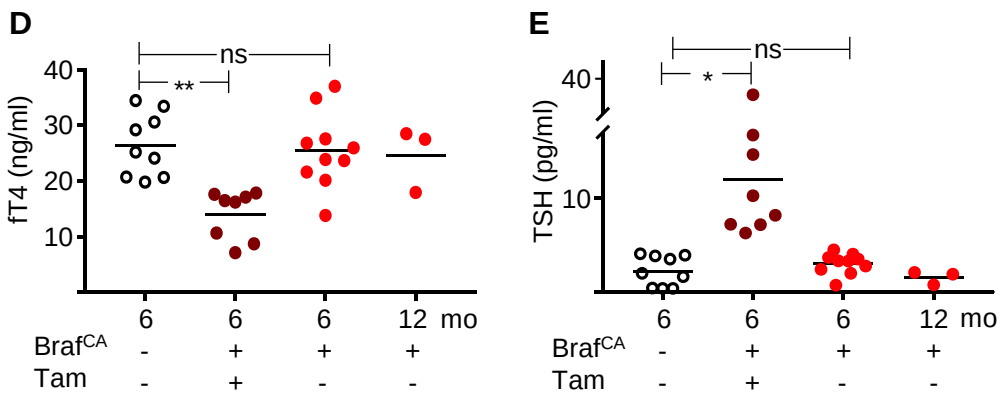

Fig. S3. Effects of induced *Braf*^{CA} activation in mouse thyroid. *TgCreER*^{T2}*;Braf*$^{CA/+}$ mice were injected or not with tamoxifen (tam; daily x3) after weaning. At times indicated, thyroids were excised and processed for microscopy of paraffin sections stained with hematoxylin-eosin, and peripheral blood was saved for measurements of thyroid stimulating hormone (TSH) and free thyroxin (fT4) levels. **A-C**, Cross section of right thyroid lobe in wildtype (wt) and Braf mutant mice 2 weeks (w) and 2 months (mo) after first tamoxifen injection. Note general morphological changes in mutant thyroids at both time points. la, larynx, cricoid level; e, esophagus. Scale bars: 500 µm. **DE**, Mean and individual circulating free T4 (fT4) and TSH levels in mutant mice with tamoxifen-induced or spontaneous (non-induced) Cre activation. Dots represent individual values. *, p=0.005; **, p=0.005. ns, not significant.

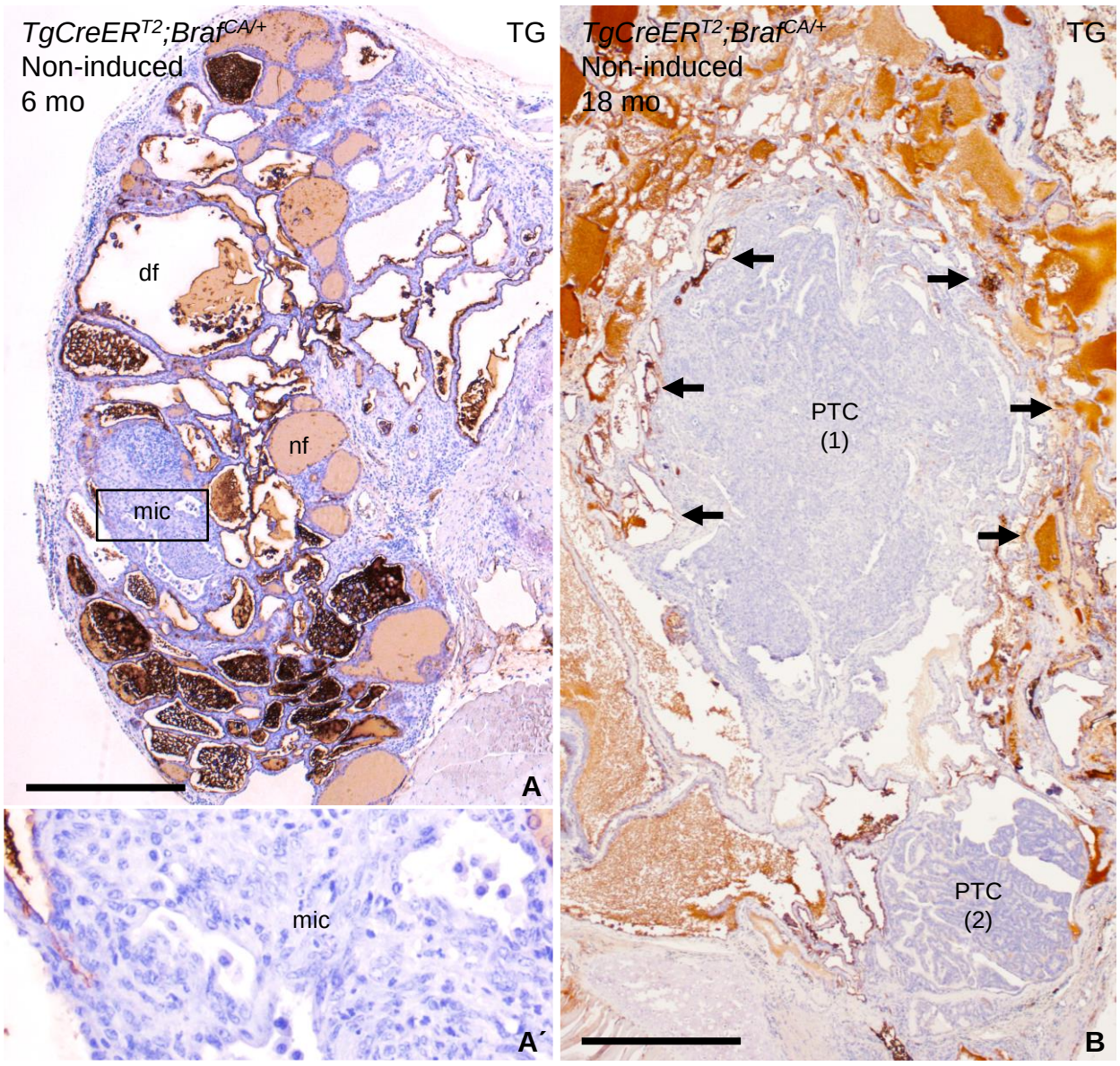

Fig. S4. Dedifferentiation of papillary thyroid carcinomas (PTC) in non-induced *TgCreER^{T2};Braf$^{CA/+}$* mice. Images with mmunohistochemical staining of thyroglobulin (TG). **A**, Overview of right thyroid lobe in a 6 months mutant mouse. The tissue consists mainly of TG positive (TG+) follicles with homogeneous or disrupted colloid and a microcarcinoma (mic) entirely free of TG immunoreactivity. A´ shows high power of boxed area. nf, normal follicle; df, dilated follicle. **B**, Advanced tumor stage in an 18 month old mutant. Image from a parallel section to that shown in Fig. 1I. Only the two carcinomas (1 and 2) are devoid of TG; TG+ follicles are present in the marginal zone of tumors (arrows). Scale bars (A, B): 500 µm.

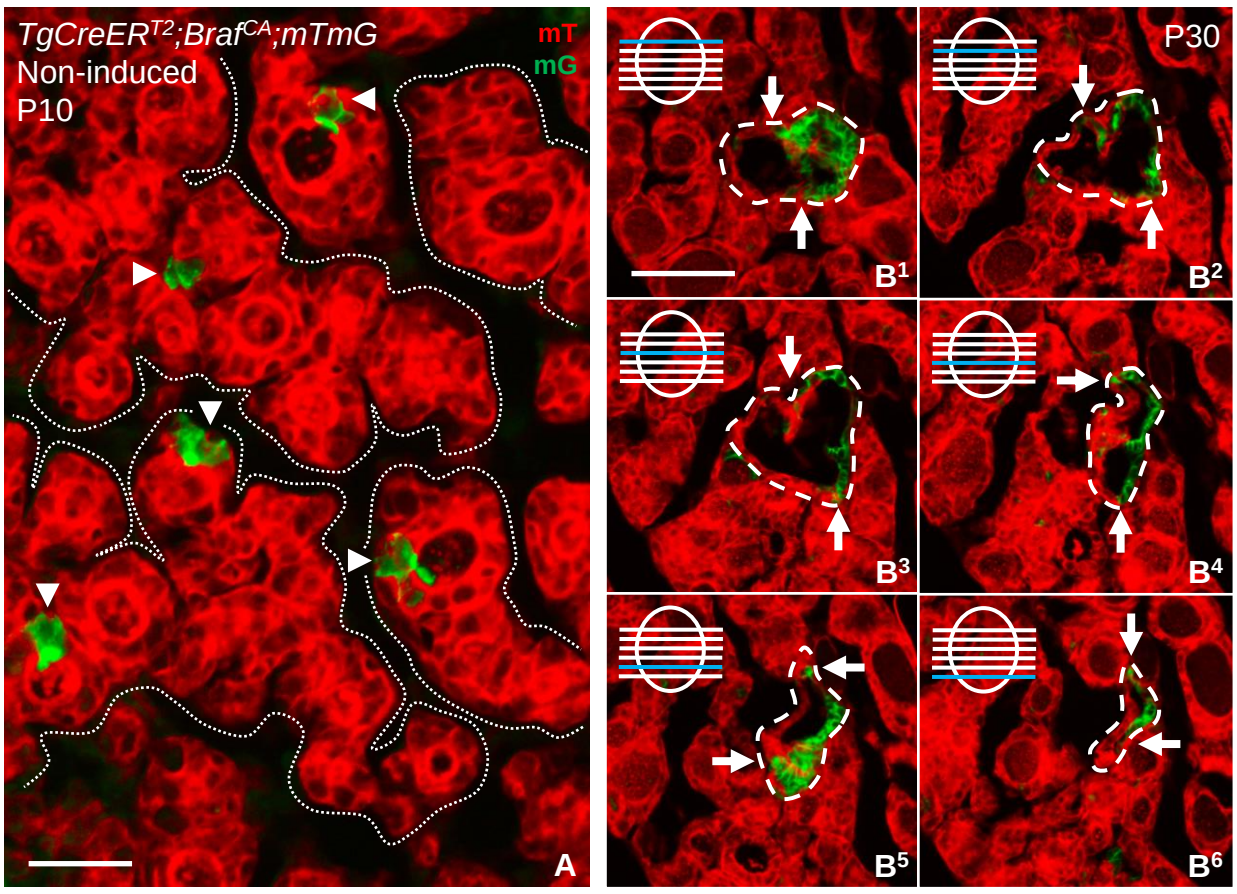

Fig. S5. Tracing spontaneous *Braf*^{CA} activation and clonal development of Braf mutant cells in the postnatal thyroid gland. *TgCreER*^{T2}*; Braf*$^{CA/+}$ mice were recombined with the double fluorescent *mTmG* reporter to generate *TgCreER*^{T2}*; Braf*$^{CA/+}$*;mTmG* mice. **A**, Incidence of *mTmG* activation as revealed at postnatal day 10 (P10). Arrowheads indicate single mG^{+} follicle cells present in premature follicles. Branching network of parenchyma is outlined (dotted lines). **B**, Serial sections (B$^{1\text{-}6}$) of an enlarged, dual labeled (compound mT^{+}/mG^{+}) follicle with an irregular, abnormal shape (encircled). Section levels with reference to the enlarged follicle are indicated in upper, left corner; B^{3} is identical to Fig. 4H. Note the follicle consists of two differentially labeled, contiguous epithelial domains of equal size. Arrows indicate transition sites of mT^{+} and mG^{+} clones. Scale bars: 100 (B) and 25 (A) µm.

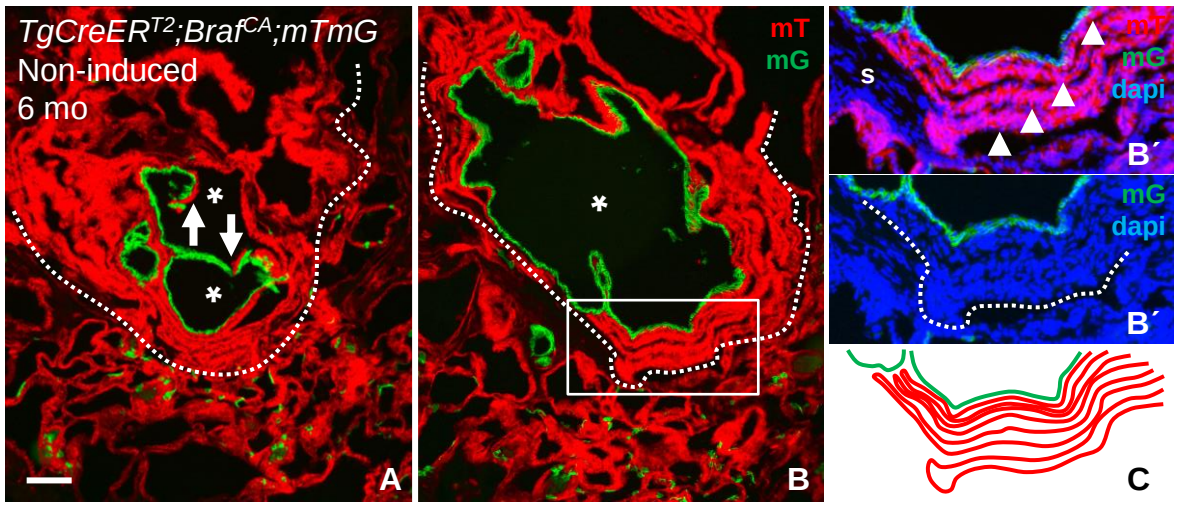

Fig. S6. Clonal selection of growth in papillary thyroid carcinogenesis following stochastic *Braf*^{CA} activation. Thyroid tissue from a 6 month (mo) old *TgCreER*^{T2}*;Braf*$^{CA/+}$*;mTmG* mouse. **A, B**, Serial images of a dual labeled tumor (encircled) indicating predominant papillary growth of a mT^{+} clone entrapping a mG^{+} clone that essentially faces the enlarged lumen (asterisks). Arrows indicate clonal transition sites of the originating oligoclonal epithelium. B´ show boxed area in B with additional dapi staining illustrating multilayered folding (arrowheads) of the mT^{+} neoplastic epithelium. **C**, Cartoon of B´ for clarity. s, stromal tissue surrounding tumor. Scale bar: 100 µm.

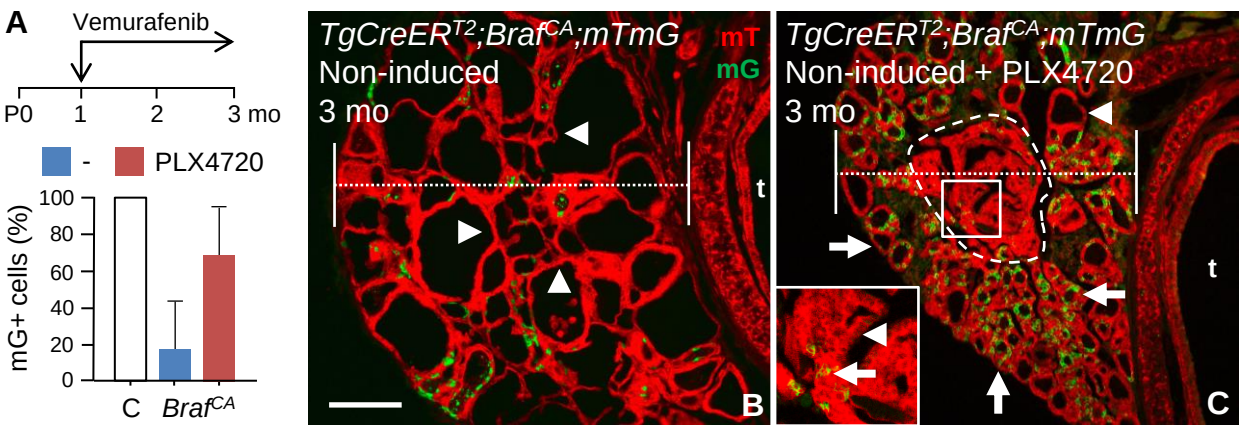

Fig. S7. Resistance of tumorigenic clones to Braf^{V600E} kinase inhibition. *TgCreER^{T2};Braf$^{CA/+}$;mTmG* mice were fed PLX4720 (417 ppm) from weaning and sacrificed at 3 months of age. Serial sections were counted for mG^{+} thyroid cells and compared to that of age-matched *TgCreER^{T2};mTmG* mice. **A**, Maintained reporter gene activation in drug-treated mutants. Mean±sd (n): controls (6), untreated mutants (6), tamoxifen-treated mutants (6); three section levels/gland. **B, C**, Normalization of lobe size (indicated by brackets), follicle size and mG^{+} labeling of cells by vemurafenib. Note preserved mT+ labeling of microcarcinoma cells (encircled). Inset shows boxed area in C. Arrows, G^{+} cells; arrowheads, mT^{+} cells; t, trachea. Scale bar: 200 µm.